ELKS1 localizes the synaptic vesicle priming protein bMunc13-2 to a specific subset of active zones

Hiroshi Kawabe,[1] Miso Mitkovski,[2] Pascal S. Kaeser,[4,5] Johannes Hirrlinger,[3,6] Felipe Opazo,[7,8] Dennis Nestvogel,[1] Stefan Kalla,[1] Anna Fejtova,[9,10,11] Sophie E. Verrier,[12] Simon R. Bungers,[1] Benjamin H. Cooper,[1] Frederique Varoqueaux,[1] Yun Wang,[13] Ralf B. Nehring,[14,15] Eckart D. Gundelfinger,[9] Christian Rosenmund,[16] Silvio O. Rizzoli,[7] Thomas C. Südhof,[4] Jeong-Seop Rhee,[1] and Nils Brose[1]

[1]Department of Molecular Neurobiology, Center for Nanoscale Microscopy and Molecular Physiology of the Brain, [2]Light Microscopy Facility, and [3]Department of Neurogenetics, Max Planck Institute of Experimental Medicine, 37075 Göttingen, Germany
[4]Department of Molecular and Cellular Physiology, Howard Hughes Medical Institute, Stanford University School of Medicine, Stanford, CA 94305
[5]Department of Neurobiology, Harvard Medical School, Boston, MA 02115
[6]Carl Ludwig Institute for Physiology, University of Leipzig, 04109 Leipzig, Germany
[7]Department of Neuro- and Sensory Physiology and [8]Center for Biostructural Imaging of Neurodegeneration, University of Göttingen Medical Center, 37073 Göttingen, Germany
[9]Department of Neurochemistry and Molecular Biology, Leibniz Institute of Neurobiology, 39118 Magdeburg, Germany
[10]Research Group Presynaptic Plasticity, Leibniz Institute of Neurobiology and Center for Behavioral Brain Sciences, Otto von Guericke University, 39106 Magdeburg, Germany
[11]Department of Psychiatry and Psychotherapy, University Hospital, Friedrich Alexander University Erlangen-Nuremberg, 91054 Erlangen, Germany
[12]Department of Neurobiology, Max Planck Institute for Biophysical Chemistry, 37077 Göttingen, Germany
[13]Department of Neuroscience, University of Texas Southwestern Medical Center, Dallas, TX 75390
[14]Department of Molecular and Human Genetics and [15]Department of Neuroscience, Baylor College of Medicine, Houston, TX 77030
[16]Neuroscience Research Centre and NeuroCure, Charité, University Medicine Berlin, 10117 Berlin, Germany

Presynaptic active zones (AZs) are unique subcellular structures at neuronal synapses, which contain a network of specific proteins that control synaptic vesicle (SV) tethering, priming, and fusion. Munc13s are core AZ proteins with an essential function in SV priming. In hippocampal neurons, two different Munc13s—Munc13-1 and bMunc13-2—mediate opposite forms of presynaptic short-term plasticity and thus differentially affect neuronal network characteristics. We found that most presynapses of cortical and hippocampal neurons contain only Munc13-1, whereas ∼10% contain both Munc13-1 and bMunc13-2. Whereas the presynaptic recruitment and activation of Munc13-1 depends on Rab3-interacting proteins (RIMs), we demonstrate here that bMunc13-2 is recruited to synapses by the AZ protein ELKS1, but not ELKS2, and that this recruitment determines basal SV priming and short-term plasticity. Thus, synapse-specific interactions of different Munc13 isoforms with ELKS1 or RIMs are key determinants of the molecular and functional heterogeneity of presynaptic AZs.

Introduction

Neurotransmitter release at synapses is spatially restricted to the active zone (AZ) compartment of axon terminals, where synaptic vesicle (SV) docking, priming, and Ca^{2+}-triggered fusion take place in a spatially and temporally highly coordinated manner (Wojcik and Brose, 2007; Südhof, 2012). AZ proteins control SV docking, priming, and fusion. They include (a) the coiled-coil domain proteins ELKS (glutamic acid/leucine/lysine/serine-rich protein; also called Rab6IP2, CAST [cytomatrix of the AZ-associated structural protein], or ERC [ELKS/Rab6IP2/CAST family protein]; Monier et al., 2002; Ohtsuka et al., 2002; Wang et al., 2002; Deguchi-Tawarada et al., 2004); (b) Rab3-interacting proteins (RIMs; Wang et al., 1997), which are Rab3 effector proteins that regulate synaptic transmitter release and long-term synaptic plasticity (Castillo et al., 2002; Schoch et al., 2002, 2006; Calakos et al., 2004; Kiyonaka et al., 2007; Han et al., 2011; Kaeser et al., 2011; Fernández-Busnadiego

Correspondence to Nils Brose: brose@em.mpg.de

S. Kalla's present address is Accenture GmbH, D-40221 Düsseldorf, Germany.

S.E. Verrier's present address is United BioSource Corporation, London W6 7HA, England, UK.

S.R. Bungers' present address is labfolder GmbH, 10247 Berlin, Germany.

F. Varoqueaux's present address is Dept. of Fundamental Neurosciences, University of Lausanne, 1015 Lausanne, Switzerland.

Abbreviations used: AZ, active zone; CAST, cytomatrix of the AZ-associated structural protein; DIV, day in vitro; DKO, double KO; EPSC, excitatory postsynaptic current; FRET, Förster resonance energy transfer; GAD, Gal4 transcriptional activation domain; GBD, Gal4 DNA-binding domain; KI, knock-in; KO, knockout; MBP, maltose-binding protein; RabGDI, Rab GDP dissociation inhibitor; RIM, Rab3-interacting protein; RRP, readily releasable vesicle pool; SV, synaptic vesicle; WT, wild type; YTH, yeast two hybrid.

The Rockefeller University Press $30.00
J. Cell Biol. Vol. 216 No. 4 1143–1161
https://doi.org/10.1083/jcb.201606086

et al., 2013); (c) Munc13s (Augustin et al., 1999a,b), which are essential SV priming proteins (Augustin et al., 1999b; Varoqueaux et al., 2002); and the scaffold proteins (d) Piccolo/Aczonin, (e) Bassoon (tom Dieck et al., 1998; Wang et al., 1999; Fenster et al., 2000), and (f) α-Liprins (Serra-Pagès et al., 1998; Zürner and Schoch, 2009; Spangler et al., 2013). All known AZ proteins contain sites for mutual binding, leading to multivalent interactions that result in a complex AZ protein network (Betz et al., 2001; Ohtsuka et al., 2002; Schoch et al., 2002; Wang et al., 2002; Takao-Rikitsu et al., 2004).

The Munc13 proteins Munc13-1, ubMunc13-2, bMunc13-2, and Munc13-3 are encoded by three genes (*Unc13A*/*Unc13B*/*Unc13C*). Munc13-1 and ubMunc13-2 have evolutionarily conserved structures, including (a) an N terminus with a C_2 domain (C_2A) and a Ca^{2+}/CaM-binding site, (b) a central tandem arrangement of a diacylglycerol and phorbol ester–binding C_1 domain and a second C_2 domain (C_2B), and (c) a C terminus with a Munc13 homology or minimal Munc13 priming domain and a third C_2 domain (C_2C). bMunc13-2, a variant of Munc13-2 generated by a specific promoter and alternative splicing, and Munc13-3 carry unrelated N termini, followed by central and C-terminal parts that are conserved in all Munc13s (Brose et al., 1995; Koch et al., 2000; Betz et al., 2001; Basu et al., 2005; Stevens et al., 2005). Munc13s are essential SV priming proteins. Knockout (KO) of all Munc13s in mouse neurons results in a complete loss of fusogenic readily releasable SVs and a total block of spontaneous and evoked synaptic transmission (Varoqueaux et al., 2002). The priming function of Munc13s is thought to be because of their ability to regulate the conformation of the t-SNAREs Syntaxin 1 and Syntaxin 2 (Richmond et al., 2001; Ma et al., 2013; Yang et al., 2015).

The AZ-specific localization of different Munc13s and their functional characteristics are thought to be key determinants of the AZ restriction of transmitter release, the speed of excitation secretion coupling, and short-term plasticity features of individual synapses (Rosenmund et al., 2003). That different Munc13s can determine different forms of short-term synaptic plasticity is illustrated by studies on genetically manipulated cultured glutamatergic hippocampal neurons. If such neurons are engineered to contain only Munc13-1, they exhibit short-term depression during high-frequency stimulation as their main short-term plasticity feature. In contrast, expression of bMunc13-2 or ubMunc13-2, which are the remaining Munc13 variants in Munc13-1 KO neurons, leads to frequency facilitation and strong augmentation (Rosenmund et al., 2002). The differential short-term plasticity features of different Munc13s reflect protein-intrinsic functional differences (Rosenmund et al., 2002) and are regulated by Ca^{2+}/CaM binding, diacylglycerol binding, and Ca^{2+}/phospholipid binding to the corresponding regulatory domains (Rhee et al., 2002; Rosenmund et al., 2002; Junge et al., 2004; Zikich et al., 2008; Shin et al., 2010).

Interestingly, Munc13s not only differ with regard to the short-term plasticity features they determine but also can be targeted to different synapse subpopulations. First corresponding evidence was obtained in studies on mature cultured glutamatergic hippocampal neurons, which express Munc13-1, bMunc13-2, and ubMunc13-2. KO of Munc13-1 in these neurons, which normally exhibit short-term depression during high-frequency stimulation caused by the dominant expression of Munc13-1, leads to a total shutdown of the majority of synapses. Some 10% of the synapses remain normally active but show frequency facilitation during and strong augmentation after high-frequency stimulation. This indicates that SV priming in most synapses of hippocampal neurons is mediated solely by Munc13-1, whereas only a small synapse subpopulation (∼10%) uses bMunc13-2 or ubMunc13-2 (Augustin et al., 1999b; Varoqueaux et al., 2002). Such differential equipment of synapses with different Munc13s, conveying different short-term plasticity characteristics, may allow for target cell–specific synaptic signaling and broad bandwidth signal propagation in vivo and thus determine unique neuronal network characteristics (Rosenmund et al., 2002).

The mechanisms that mediate the differential AZ targeting of Munc13 isoforms likely involve their different N termini. Munc13-1 and ubMunc13-2 bind to the Zn^{2+}-finger domain of the AZ proteins RIM1α, RIM1β, and RIM2α via their conserved N-terminal C2 domains (Betz et al., 2001; Dulubova et al., 2005; Andrews-Zwilling et al., 2006; Kaeser et al., 2008). RIMs play a crucial role in the control of synaptic transmitter release and presynaptic forms of long-term potentiation. RIM1α KO and RIM1/2 double KO (DKO) neurons exhibit reduced SV priming and altered short-term synaptic plasticity (Calakos et al., 2004; Kaeser et al., 2011), which is reminiscent of the phenotype seen in Munc13-1–deficient neurons (Augustin et al., 1999b; Rosenmund et al., 2002). Interference with Munc13/RIM binding perturbs SV priming (Betz et al., 2001; Dulubova et al., 2005; Deng et al., 2011), indicating that this interaction has a regulatory function in SV priming and that the two proteins act in the same presynaptic regulatory pathway. This notion is supported by the findings that Munc13-1 and ubMunc13-2 levels are reduced in the brains of RIM KO mice (Schoch et al., 2002; Andrews-Zwilling et al., 2006; Deng et al., 2011), that RIM binding influences the AZ recruitment of Munc13-1 (Andrews-Zwilling et al., 2006), and that RIM binding disrupts Munc13-1 and ubMunc13-2 homodimerization, leading to the activation of the SV priming function of Munc13-1 and ubMunc13-2 (Deng et al., 2011). The AZ recruitment of Munc13-1 and ubMunc13-2 seems to be evolutionarily conserved, as RIM-binding is sufficient for recruitment of *Caenorhabditis elegans* Unc-13 to the AZ (Hu et al., 2013). *Drosophila melanogaster* Unc13s, on the other hand, have unique N-terminal structures (Böhme et al., 2016). Likewise, the Munc13-2 splice variant bMunc13-2 has an N-terminal sequence that lacks a RIM-binding site and is not related to mammalian Munc13-1 and ubMunc13-2 or to any Unc-13/Unc13 variants in *C. elegans* or *Drosophila* (Brose et al., 1995; Betz et al., 2001), indicating that proteins other than RIMs must be involved in the AZ targeting and regulation of bMunc13-2.

We show here that the AZ protein ELKS1 is involved in the presynaptic recruitment and anchoring of bMunc13-2. ELKS1 belongs to the ELKS family of AZ proteins, which are encoded by two genes, *ERC1* and *ERC2* (Nakata et al., 1999; Ohtsuka et al., 2002; Wang et al., 2002; Kaeser et al., 2009). ELKSs form complexes with RIMs at AZs, directly interact with Bassoon, Piccolo (Takao-Rikitsu et al., 2004), and Liprin-α (Ko et al., 2003), and are thought to contribute to and regulate an AZ protein scaffold that provides a platform for the SV priming machinery (Hagiwara et al., 2005; Siksou et al., 2007). The physiological roles of ELKSs in neurons are complex and may differ between orthologues of different species. For example, elimination of the *Drosophila* ELKS orthologue Bruchpilot (Brp), which contains an evolutionarily unique C terminus, results in the disruption of the T-bar structure at presynaptic

AZs, impaired neurotransmitter release, and mislocalization of overexpressed Ca^{2+} channels (Kittel et al., 2006; Wagh et al., 2006). In contrast, elimination of *C. elegans* ELKS has only mild phenotypic consequences (Deken et al., 2005), although it is required for the expression of a gain-of function mutant form of its interactor Syd2/Liprin (Dai et al., 2006), and deletion of both ELKS genes in mice leads to decreased neurotransmitter release through distinct mechanisms at different synapses. At hippocampal inhibitory synapses, ELKSs boost presynaptic Ca^{2+} influx to enhance transmitter release probability (Liu et al., 2014), whereas at excitatory synapses, ELKS removal impairs SV priming (Held et al., 2016). Deletion of ELKS2/CAST alone has multiple but rather mild consequences, including an increase of the pool of primed and readily releasable vesicles (RRP) SVs at hippocampal inhibitory synapses (Kaeser et al., 2009), altered AZ structure in ribbon synapses (tom Dieck et al., 2012), and altered SV recycling at AZs in sympathetic superior cervical ganglion neurons (Mochida et al., 2016). Our study characterizes a novel AZ targeting and anchoring mechanism for bMunc13-2 that is mediated specifically by ELKS1 and that recruits bMunc13-2 to a small subset of synaptic terminals in hippocampal neurons.

Results

Differential subcellular distribution of Munc13-1 and bMunc13-2

Previous electrophysiological studies on genetically engineered hippocampal glutamatergic neurons provided indirect evidence for the notion that only some 10% of synapses in these cells operate with Munc13-2 (Rosenmund et al., 2002; Varoqueaux et al., 2002). To obtain direct evidence for such synapse-specific Munc13-2 recruitment, we studied the expression and localization of bMunc13-2 and ubMunc13-2 in knock-in (KI) mutant mice (Munc13-2^{EYFP}) expressing C-terminally EYFP-tagged Munc13s (Kalla et al., 2006; Cooper et al., 2012). In a first set of experiments, we analyzed the relative expression levels of ubMunc13-2–EYFP (200 kD predicted molecular weight) and bMunc13-2–EYFP (240 kD predicted molecular weight) in cultured primary hippocampal neurons from Munc13-2^{EYFP} KI mice (Cooper et al., 2012). Proteins were separated by SDS-PAGE along with recombinantly expressed ubMunc13-2–EGFP and bMunc13-2–EGFP and analyzed by Western blotting with anti-GFP antibodies and isoform-specific antibodies. We found that bMunc13-2–EYFP predominates among Munc13-2–EYFP proteins from Munc13-2^{EYFP} mouse hippocampal neurons (bMunc13-2–EYFP:ubMunc13-2-EYFP ratio of 4.5:1; Fig. 1 A). Similar results were obtained with lysates of hippocampal tissue from Munc13-2^{EYFP} KI mice (bMunc13-2–EYFP:ubMunc13-2–EYFP ratio of 6:1; Fig. 1 A). To compare the subcellular distributions of Munc13-1 and bMunc13-2, we immunostained cultured autaptic hippocampal neurons of Munc13-2^{EYFP} mice using a rabbit polyclonal anti-GFP antibody, a guinea pig polyclonal antibody to Munc13-1, and a mouse monoclonal antibody to Bassoon (Fig. 1, B and C). Corresponding analyses of Munc13-1– and Bassoon-positive puncta, which mostly represent AZs, showed that 77% were devoid of Munc13-2–EYFP whereas only 23% also contained Munc13-2–EYFP (Fig. 1).

These data show that bMunc13-2 is the dominant Munc13-2 splice variant in the mouse hippocampus and that only a subset of synapses in single, cultured, hippocampal neurons are enriched with bMunc13-2.

bMunc13-2 binds ELKS1

The entire primary sequences of mammalian Munc13-1 and ubMunc13-2 and *C. elegans* Unc-13-LR are homologous, including an N-terminal RIM-binding domain (Betz et al., 2001; Andrews-Zwilling et al., 2006). In contrast, bMunc13-2 and Munc13-3 contain unrelated N termini, except for a short coiled-coil motif that is 52% identical between bMunc13-2 and Munc13-3 and conserved from fish to human (Fig. 2 A) but is not present in *Drosophila* (Böhme et al., 2016). This indicates a unique role of the N termini of bMunc13-2 and Munc13-3.

To identify proteins that bind to the bMunc13-2 N terminus and might recruit bMunc13-2 to a defined subpopulation of AZs, we performed yeast two-hybrid (YTH) screens using a mouse embryo cDNA prey library, encoding Gal4 transcriptional activation domain (GAD) fusion proteins, with the bait construct pGBDC2-bMunc13-2(1–605), which encodes a fusion protein consisting of the Gal4 DNA-binding domain (GBD) in frame with residues 1–605 of bMunc13-2, GBD-bMunc13-2(1–605). We isolated 13 positive clones, 8 of which encode the C terminus of ELKS1, including its C-terminal coiled-coil domain, GAD-ELKS1(771–976) (Fig. 2 A). Like the corresponding region in ELKS2/CAST, this region of ELKS1 binds to RIMs via its C-terminal PDZ binding domain (Ohtsuka et al., 2002; Wang et al., 2002). Two other bait constructs containing the N-terminal coiled-coil motif of bMunc13-2, GBD-bMunc13-2(1–305) and GBD-bMunc13-2(70–605), bound to GAD-ELKS1(771–976) (Fig. 2 B), whereas two bait constructs lacking the coiled-coil domain, GBD-bMunc13-2(188–605) and GBD-bMunc13-2(1–605Δ145–187), did not.

These data show that the N-terminal coiled-coil domain of bMunc13-2 (residues 145–187) interacts with the C terminus of ELKS1 containing its C-terminal coiled-coil domain.

Because Munc13-3 contains an N-terminal coiled-coil domain that is homologous to the ELKS1-binding domain of bMunc13-2, we tested if Munc13-3 also binds to ELKS1. However, a bait construct containing residues 1–304 of Munc13-3, GBD-Munc13-3(1–304), did not interact with GAD-ELKS1(771–976) (Fig. 2 B). This was confirmed in subsequent biochemical assays (not depicted) and indicates that bMunc13-2 and ELKS1 interact very specifically, whereas Munc13-3 may have other binding partners.

To verify our YTH data and study the isoform specificity of the bMunc13-2–ELKS interaction, we performed cosedimentation experiments. We purified GST fusion proteins of ELKS1, GST-ELKS1(771–976), or a corresponding fragment of ELKS2, GST-ELKS2(751–969), immobilized them on glutathione Sepharose beads, and examined their interaction with a purified maltose-binding protein (MBP) fusion protein of bMunc13-2, MBP-bMunc13-2(1–305). We found that only GST-ELKS1(771–976), but not GST-ELKS2(751–969), bound MBP-bMunc13-2(1–305) in a stoichiometric manner. Neither MBP nor GST alone interacted with GST-ELKS1(771–976) or MBP-bMunc13-2(1–305) (Fig. 2, C and D).

To test whether the interaction between ELKS1(771–976) and bMunc13-2(70–204) occurs within cells, we measured Förster resonance energy transfer (FRET) between EYFP and ECFP fusion proteins in live hippocampal neurons at 6 d in vitro (DIV), when hardly any synapses are formed yet and neither full-length bMunc13-2 nor ELKSs are yet recruited

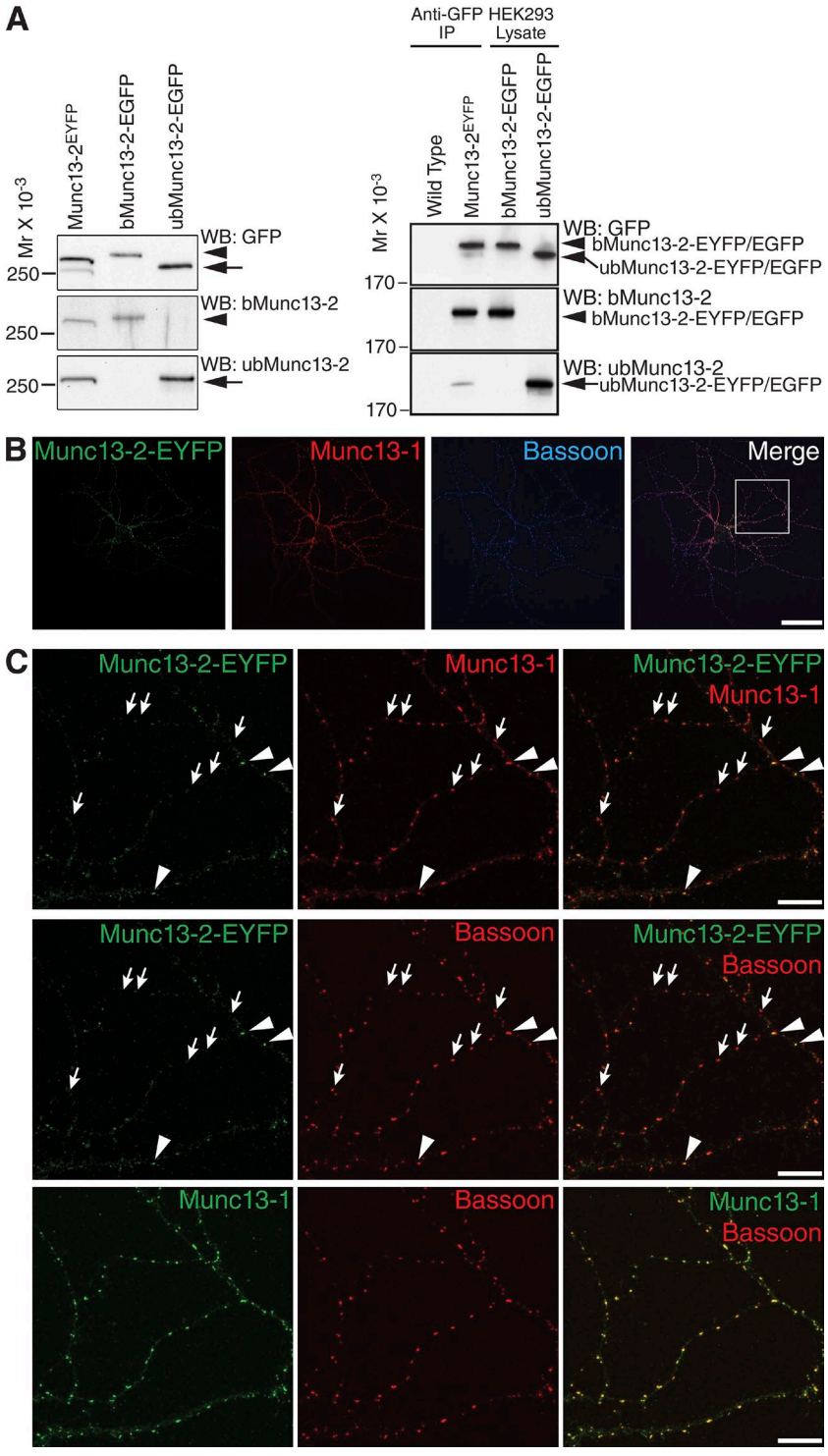

Figure 1. **Differential expression and subcellular localization of Munc13-2 variants in mouse hippocampal neurons.** (A) bMunc13-2 and ubMunc13-2 expression levels in mouse hippocampal neurons. (Left) EYFP-fused Munc13-2 isoforms were extracted from cultured hippocampal neurons of Munc13-2^{EYFP} KI mice. (Right) EYFP-fused Munc13-2 isoforms were immunoprecipitated from detergent extracts of hippocampal synaptosomes from Munc13-2^{EYFP} KI mice. Extracted proteins or immunoprecipitates (IP) were separated by SDS-PAGE along with recombinant bMunc13-2–EGFP and ubMunc13-2–EGFP (right two lanes) and analyzed by Western blotting (WB) with anti-GFP (top), anti–bMunc13-2 (middle), and anti–ubMunc13-2 (bottom) antibodies. Two GFP-positive bands appeared in samples from Munc13-2^{EYFP} KI hippocampal neurons (left) and from hippocampal tissue (right), whose molecular weights corresponded to those of recombinant bMunc13-2–EGFP (arrowheads) and ubMunc13-2–EGFP (arrows), respectively. The band with larger molecular weight cross-reacted with the anti–bMunc13-2 antibody, whereas the one with lower molecular weight cross-reacted with the anti–ubMunc13-2 antibody. By densitometric quantification of GFP signals on films using ImageJ, ratios of over 4.5:1 and 6:1 were determined between expression levels of bMunc13-2–EYFP and ubMunc13-2–EYFP in Munc13-2^{EYFP} KI neurons and in hippocampal tissues, respectively. (B and C) Subcellular localization of Munc13-2 in mouse hippocampal neurons. Cultured autaptic hippocampal neurons from Munc13-2^{EYFP} KI mice were immunostained for Munc13-1, EYFP, and Bassoon. (B) The overview image of an autaptic neuron shows that AZs containing Munc13-1 only (red) are much more abundant than AZs containing Munc13-2–EYFP (green). Bar, 50 µm. (C) A high-magnification image of the boxed image section in B shows some AZs containing Munc13-1 and Munc13-2–EYFP (arrowheads) among numerous AZs containing only Munc13-1 (arrows). Only 23% of puncta double positive for Munc13-1 and Bassoon were also enriched for Munc13-2–EYFP (n = 1,942 synapses, n = 12 images). Bars, 10 µm.

to AZs. Single-cell FRET measurements showed significant FRET signals generated by ECFP-bMunc13-2(70–204) and EYFP-ELKS1(771–976) (Fig. S1 A) and an increase of donor fluorescence after acceptor bleaching (Fig. S1 B). Normalized FRET values obtained for ECFP-bMunc13-2(70–204)/EYFP-ELKS1(771–976) pairs in neurons were ∼0.07 (n = 25 cells, three independent experiments; Fig. S1 C). This value is significantly higher (approximately sevenfold) than the FRET value obtained in cells coexpressing soluble ECFP and EYFP and represents 15% of the FRET signal (0.46 ± 0.04, n = 15 cells, three independent experiments) measured when the two fluorescent protein moieties are linked by a 15–amino acid spacer (Fig. S1 C). The FRET intensity seen with ECFP-bMunc13-2(70–204)/EYFP-ELKS1(771–976) pairs is similar to the one observed with SNARE proteins (Verrier et al., 2008).

Our YTH, biochemical, and FRET data indicate that bMunc13-2 and ELKS1 interact directly, specifically, stoichiometrically, and within cells.

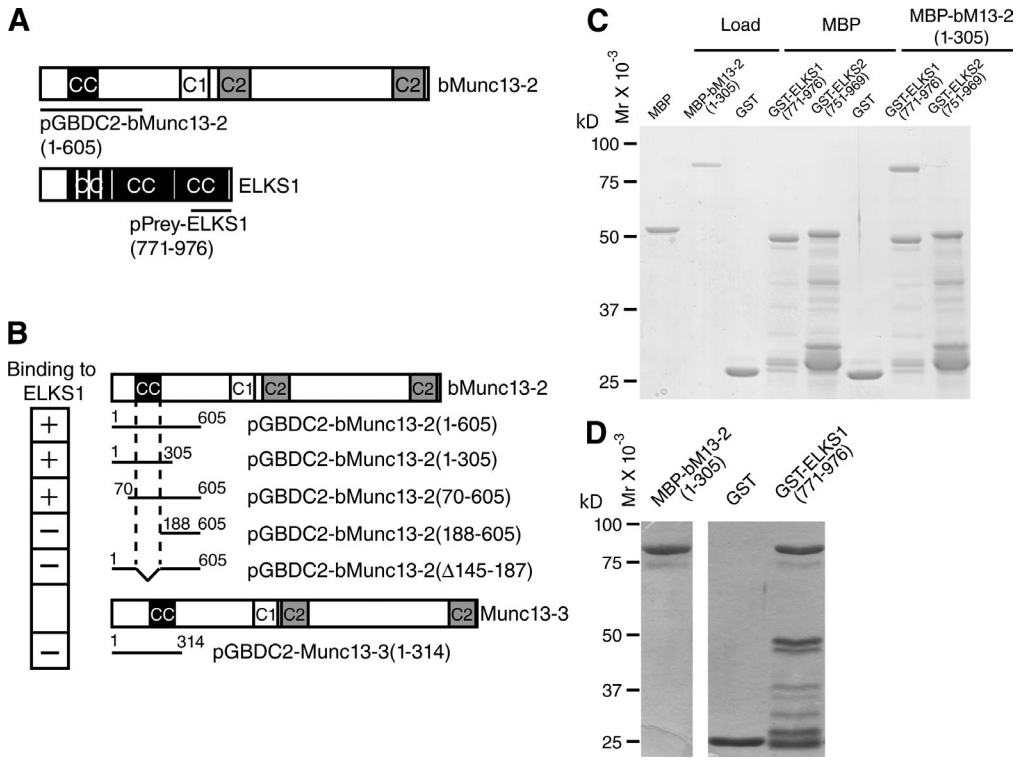

Figure 2. **bMunc13-2 and ELKS1 form a protein complex.** (A) Domain structures of bMunc13-2 and ELKS1. The sequences covered by the bait vector pGBDC2-bMunc13-2(1–605) and the bMunc13-2–binding ELKS1 prey clone pGAD-ELKS1(771–976) obtained in the YTH screen are indicated. Coiled-coil motifs were predicted by COILS/PCOILS. CC, coiled coil motif; C1, C_1 domain; C2, C_2 domain. (B) The ELKS1 binding site in bMunc13-2 maps to the coiled-coil motif in the N terminus. Shown are the domain structures of bMunc13-2 and Munc13-3 and the representations of bait vectors used in YTH binding assays with the ELKS1 prey vector pGAD-ELKS1(771–976). (C) Isoform-specific binding of MBP-bMunc13-2(1–305) to GST-ELKS1 (771–976), but not to GST-ELKS2(751–969), in cosedimentation assays. Proteins that bound to immobilized GST-ELKS1(771–976) were subjected to SDS-PAGE and stained with Coomassie Brilliant blue. Note that MBP-bMunc13-2(1–305) bound to GST-ELKS1(771–976) robustly, whereas binding to GST-ELKS2(751–969) was not detectable. Data are representative of three independent experiments. (D) Stoichiometric interaction of MBP-bMunc13-2(1–305) and GST-ELKS1(771–976). A 3.5× higher amount of MBP-bMunc13-2(1–305), 0.14 mg/ml, was loaded to the GST-ELKS1(771–976) affinity matrix than in the assay shown in C. Absorbance units of Coomassie Brilliant blue–stained MBP–bMunc13-2(1–305) versus GST-ELKS1(771–976) in this experiment were 12,056:11,428. Given that the molecular weights of the two proteins are ∼80 kD and ∼45 kD, MBP-bMunc13-2(1–305) and GST-ELKS1(771–976) are interacting with an apparent 1:1.69 stoichiometry. The image of loaded MBP-bMunc13-2(1–305) (left) is from the same SDS-PAGE gel as the one for stoichiometric interaction (right). Data are representative of two independent experiments.

bMunc13-2 is preferentially accumulated at ELKS1-enriched synapses

Given that only ELKS1 and not ELKS2 binds to bMunc13-2 (Fig. 2), and in view of the fact that cultured hippocampal neurons enrich only a subset of synapses with bMunc13-2 (Fig. 1 C), we next tested whether bMunc13-2 is differentially associated with ELKS1 containing synapses in brain tissue. We immunostained brain sections of wild-type (WT) mice and of Munc13-2 KO, ELKS2 KO, and conditional ELKS1 KO mice (ELKS1$^{f/f}$;Emx1-Cre) as negative controls with antibodies to bMunc13-2, ELKS1, ELKS2, and Bassoon (Figs. 3, S2, and S3). In ELKS1$^{f/f}$;Emx1-Cre mice, which show no obvious phenotypic changes in the cage environment, ELKS1 expression is shut down in cortical and hippocampal neurons and glia cells (Gorski et al., 2002). Prominent punctate bMunc13-2–positive signals were detected in the cerebral cortex (Fig. 3, A and B), in the hilus of the dentate gyrus (Figs. S2 and S3), and in the stratum oriens of the hippocampal CA1 region (not depicted). In the cortex, ELKS1 signals were rather widespread but showed a very wide range of intensity and were distinctly enriched in a subset of Bassoon-positive presynapses, where bMunc13-2 was colocalized with ELKS1 (Fig. 3 A). After thresholding at a signal intensity level that was also seen at nonsynaptic sites that presumably represent partly nonspecific staining, ∼56% of ELKS1-enriched structures coincided with bMunc13-2–positive structures (Fig. 3 C), and 76% of bMunc13-2–positive structures coincided with ELKS1-enriched structures. The distribution of ELKS2, on the other hand, was unrelated to that of bMunc13-2, although most ELKS2-positive signals colocalized with Bassoon-positive AZs (Fig. 3, B and C). Very similar observations were made in the hilus of the dentate gyrus (Fig. S3).

These results show that bMunc13-2 is preferentially recruited to a subpopulation of AZs that are particularly enriched in ELKS1 as compared with ELKS2, indicating that the interaction of bMunc13-2 with ELKS1 may be the basis for the heterogeneous distribution of bMunc13-2 to distinct synapse subsets of forebrain neurons. The notion of a specific AZ enrichment of bMunc13-2 by ELKS1 is corroborated by the finding that many Munc13-1–positive synapses in autaptic hippocampal neurons contain little or no ELKS1 (Fig. S4; but see Liu et al., 2014; Held et al., 2016 for somewhat different ELKS1 distribution in mass cultures of hippocampal neurons).

The ELKS1-binding region of bMunc13-2 is required for efficient SV priming

Munc13-1/2 DKO neurons rescued with recombinant ub-Munc13-2 exhibit facilitation during and moderate (two- to threefold) augmentation after high-frequency stimulation trains

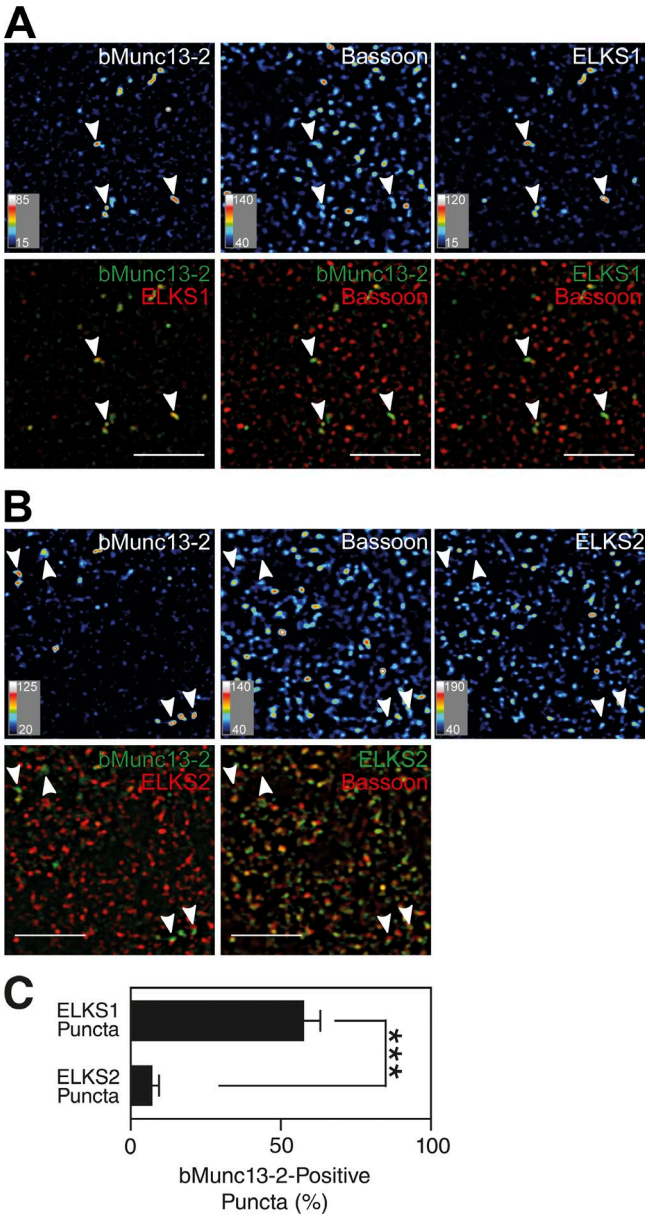

Figure 3. **bMunc13-2 is preferentially localized to ELKS1-enriched synapses.** (A and B) Localization of endogenous bMunc13-2, ELKS1, and Bassoon (A) and of bMunc13-2, ELKS2, and Bassoon (B) in the WT mouse cortex. Note that bMunc13-2 shows a similar distribution pattern to that of ELKS1 with a restriction to a limited number of synapses (arrowheads in A and B), whereas ELKS2 is accumulated in most Bassoon-positive AZs (B). Bars, 5 µm. For images represented as heat maps, quantitative score scales are presented at the bottom left of the respective image. (C) Quantification of the percentage ELKS1- and ELKS2-positive synapses containing bMunc13-2. Data are means ± SEM and were analyzed by Student's *t* test (n = 15 images; ***, P < 0.001).

(Rosenmund et al., 2002). Munc13-1 deficient hippocampal neurons, which express only Munc13-2, exhibit a similar short-term plasticity phenotype, although the degree of augmentation (7–10-fold) is higher than that observed in Munc13-1/2 DKO neurons rescued with ubMunc13-2 (two- to threefold; Rosenmund et al., 2002). In contrast to Munc13-2 driven synapses, Munc13-1–expressing synapses exhibit short-term depression during and no or very little augmentation after high-frequency stimulation (Rosenmund et al., 2002).

To study the role of bMunc13-2 and its ELKS1 interaction in SV priming and short-term plasticity, we rescued autaptic hippocampal Munc13-1/2 DKO neurons in microisland culture by overexpressing bMunc13-2–EYFP variants using the Semliki Forest virus system (Figs. 4 and S5). This rescue approach, which has been used by us in many previous studies, is particularly powerful in the context of structure–function studies on Munc13s because Munc13-1/2 DKO neurons are completely devoid of spontaneous and evoked synaptic transmitter release despite normal synaptogenesis, so that the control baseline phenotype of Munc13-1/2 DKO neurons regarding the parameters described here (Figs. 4 and S5) is "flat-line" zero (Varoqueaux et al., 2002). Immediately obvious was that neurons rescued with WT bMunc13-2-EYFP showed facilitation during and very strong augmentation after high-frequency stimulation trains. The degree of augmentation was similar to that observed in Munc13-1 KO neurons (Rosenmund et al., 2002), which mainly express bMunc13-2 (Fig. 1 A), and two to three times higher than in Munc13-1/2 DKO cells rescued with ubMunc13-2 (Junge et al., 2004; Shin et al., 2010; Fig. 4, D and E; and Fig. S5 E), indicating that bMunc13-2 is indeed the dominant Munc13-2 isoform in mature cultured hippocampal neurons (see Fig. 1 for relative bMunc13-2/ubMunc13-2 expression levels, and see three paragraphs below for more details on short-term plasticity features).

We next studied the role of ELKS1 binding to bMunc13-2 in the modulation of SV priming, synaptic strength, and synaptic plasticity. Overexpression of bMunc13-2(Δ145–187)–EYFP, which lacks the N-terminal ELKS1-binding sequence, failed to rescue synaptic transmission in ∼40% of Munc13-1/2 DKO neurons analyzed. The corresponding neurons showed no spontaneous or evoked synaptic transmission, although expression levels of bMunc13-2(Δ145–187)–EYFP were only slightly lower than the levels in functionally rescued neurons. This might indicate that levels of bMunc13-2 anchored at AZs have to pass a threshold for proper rescue activity, which is not reached in a subset of neurons if the interaction of bMunc13-2 with ELKS1 is perturbed and bMunc13-2 is not properly recruited to AZs. A similar phenotype was seen with rescue experiments using RIM binding–deficient Munc13-1 variants (Betz et al., 2001). Alternatively, a subset of neurons might use an additional, cell type–specific AZ anchoring machinery that can partly substitute for the ELKS1-mediated process (e.g., CA1 vs. CA2/CA3 pyramidal cells, as granule cells are not present in our hippocampal autaptic cultures).

Neurons expressing bMunc13-2(Δ145–187)–EYFP and showing synaptic transmission in response to an action potential exhibited strongly reduced evoked excitatory postsynaptic current (EPSC) amplitudes (0.37 ± 0.04 nA, n = 84) as compared with neurons expressing bMunc13-2–EYFP (0.83 ± 0.11 nA, n = 87, P < 0.0001; Fig. 4 A and Fig. S5, B and C). Thus, removal of the ELKS1-binding region of bMunc13-2 leads to a strong reduction of evoked EPSC amplitudes. To test whether this is caused by reduced SV priming, we estimated the size of the RRP in neurons expressing bMunc13-2–EYFP or bMunc13-2(Δ145–187)–EYFP by integrating the total charge transfer of the transient component of the EPSC response during the pulsed application of a hypertonic extracellular solution containing 0.5 M sucrose to the entire cell (Rosenmund and Stevens, 1996). RRP sizes were also significantly smaller in Munc13-1/2 DKO cells rescued with bMunc13-2(Δ145–187)–EYFP (0.10 ± 0.02 nC, n = 37) as compared with neurons

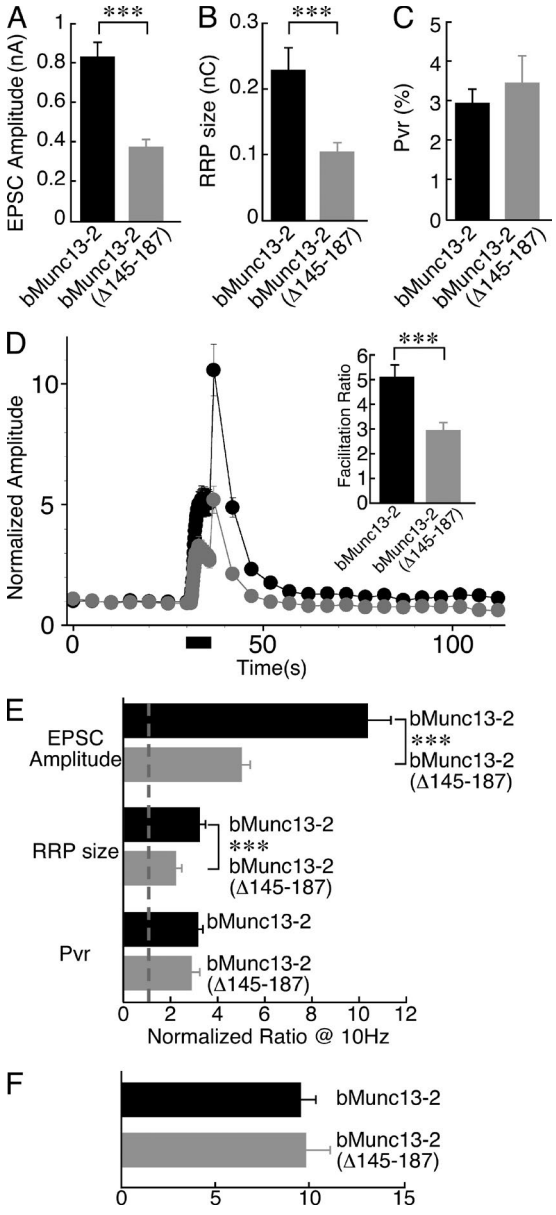

Figure 4. **ELKS1 binding of bMunc13-2 regulates synapse function.** (A) Mean evoked EPCS amplitudes in Munc13-1/2 DKO neurons expressing bMunc13-2–EYFP or bMunc13-2(Δ145–187)–EYFP. For each cell, EPSC amplitudes of 13–20 pulses at 0.2 Hz were averaged. Cells efficiently rescued with bMunc13-2(Δ145–187)–EYFP (n = 84) showed significantly smaller EPSC amplitudes than cells rescued with bMunc13-2–EYFP (n = 87). (B) Mean RRP sizes in Munc13-1/2 DKO neurons expressing bMunc13-2–EYFP or bMunc13-2(Δ145–187)–EYFP. Cells rescued with bMunc13-2(Δ145–187)–EYFP (n = 37) showed a significantly smaller RRP size than cells rescued with bMunc13-2–EYFP (n = 59). (C) Mean P_{vr} from Munc13-1/2 DKO neurons expressing bMunc13-2–EYFP or bMunc13-2(Δ145–187)–EYFP. Cells rescued with bMunc13-2(Δ145–187)–EYFP (n = 35) showed a P_{vr} similar to cells rescued with bMunc13-2–EYFP (n = 59); Student's t test, P > 0.05. (D) Short-term plasticity in Munc13-1/2 DKO neurons expressing bMunc13-2–EYFP (n = 87) or bMunc13-2(Δ145–187)–EYFP (n = 83). Neurons were initially stimulated at 0.2-Hz stimulation frequency, and then a 10-Hz train was applied for 5 s. Frequency facilitation of the EPSC was measured during the train, and augmentation was measured 1.4 s after the train. Data were normalized to the mean EPSC amplitude of the first nine data points at 0.2-Hz stimulation frequency. Munc13-1/2 DKO cells rescued with bMunc13-2(Δ145–187)–EYFP showed a significantly smaller facilitation and augmentation than cells rescued with bMunc13-2–EYFP. (E) Changes in evoked EPSC amplitudes, RRP sizes, and P_{vr} at 1.4 s after a 10-Hz stimulation train. Data are normalized to the values measured before the 10-Hz stimulation. Irrespective of the bMunc13-2 variants expressed, all three parameters are increased in the augmented state. The degree of EPSC amplitude and RRP size augmentation was significantly larger in cells expressing bMunc13-2–EYFP as compared with cells expressing bMunc13-2(Δ145–187)–EYFP (n = 83–87 for EPSC amplitude augmentation and n = 22–28 for RRP size increases), whereas the increase in P_{vr} in the augmented state was similar in the two groups (n = 11–12). (F) Similar absolute P_{vr} values at 1.4 s after a 10-Hz stimulation train in cells expressing bMunc13-2–EYFP or bMunc13-2(Δ145–187)–EYFP (n = 11–12); Student's t test, P > 0.05. Note that the ELKS1 binding–deficient construct bMunc13-2(Δ145–187)–EYFP failed to rescue synaptic transmission in ∼40% of Munc13-1/2 DKO neurons analyzed. These neurons were not included in any of the analyses shown. ***, P < 0.01, Student's t test. Data are means ± SEM.

rescued with bMunc13-2–EYFP (0.23 ± 0.03 nC, n = 59, P < 0.005; Figs. 4 B and S5 D). In accordance with the parallel changes in evoked EPSC amplitude and RRP size, Munc13-1/2 DKO neurons expressing bMunc13-2(Δ145–187)–EYFP had a vesicular release probability (P_{vr}; 3.4% ± 0.7%, n = 35) similar to neurons expressing bMunc13-2–EYFP (3.0% ± 0.4%, n = 59, P > 0.05; Fig. 4 C). Considering that bMunc13-2–EYFP and bMunc13-2(Δ145–187)–EYFP were expressed at similar levels in rescued neurons (Fig. S5 A), the differences in evoked EPSC amplitudes and RRP sizes between cells expressing bMunc13-2–EYFP or bMunc13-2(Δ145–187)–EYFP indicate that the recruitment of bMunc13-2 to the AZ by ELKS1 binding might determine the levels of bMunc13-2 at AZs and consequently SV priming activity and are consistent with a reduction of the RRP in neurons lacking ELKS1 and ELKS2 (Held et al., 2016). Alternatively, the Δ145–187 deletion might affect the intrinsic priming activity of bMunc13-2.

We next studied the short-term synaptic plasticity characteristics of Munc13-1/2 DKO neurons rescued with either bMunc13-2–EYFP or bMunc13-2(Δ145–187)–EYFP in more detail. We examined evoked EPSC amplitudes during and after a 10-Hz action potential train, normalized to the mean amplitudes obtained with seven stimuli evoked at 0.2 Hz before the 10-Hz train. Munc13-1/2 DKO neurons rescued with bMunc13-2–EYFP showed frequency facilitation during the 10-Hz train, with EPSC amplitudes increasing fivefold (5.1 ± 0.5-fold, n = 87). At 1.4 s after the 10-Hz train, neurons were again stimulated at 0.2 Hz. At this point, Munc13-1/2 DKO neurons rescued with bMunc13-2–EYFP showed a 10-fold augmentation of evoked EPSCs (10.3 ± 1.1-fold, n = 87). In contrast, Munc13-1/2 DKO neurons rescued with bMunc13-2(Δ145–187)–EYFP exhibited strongly reduced facilitation (2.9 ± 0.3-fold, n = 83, P < 0.008) and augmentation (5.0 ± 0.4-fold, n = 83, P < 0.0001; Fig. 4, D and E; and Fig. S5 E). Interestingly, the time courses of facilitation and augmentation and the augmentation/facilitation ratios were similar in cells expressing bMunc13-2–EYFP or bMunc13-2(Δ145–187)–EYFP (Fig. S5 F). Along with the reduced RRP in bMunc13-2(Δ145–187)–EYFP-expressing cells (Fig. 4 B), these data indicate that the altered short-term plasticity features of cells expressing bMunc13-2(Δ145–187)–EYFP are a direct consequence of a perturbed basal priming activity and not caused by defects in Ca^{2+}-dependent priming, which are typically seen with Munc13 variants that carry mutations in Ca^{2+}-dependent regulatory domains (Rhee et al., 2002; Junge et al., 2004; Shin et al., 2010).

We found previously that the augmentation of EPSCs in Munc13-2–driven synapses after 10-Hz stimulation trains is caused by increases of the RRP size and P_{vr} (Rosenmund et

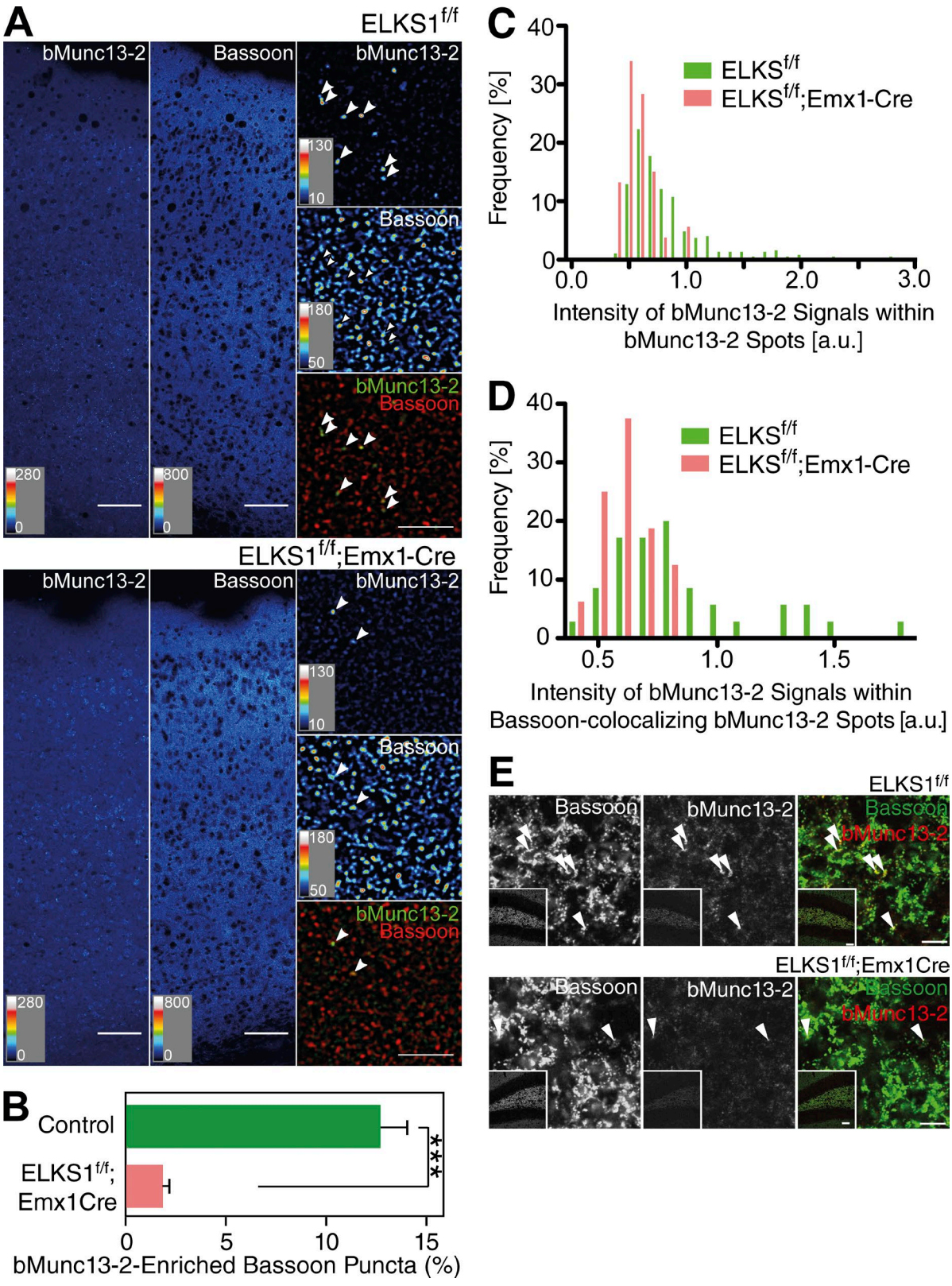

Figure 5. **AZ recruitment of bMunc13-2 depends on the presence of ELKS1.** (A) Immunohistochemical analyses of somatosensory cortex of control (ELKS1$^{f/f}$) and ELKS1 conditional KO mice (ELKS1$^{f/f}$;Emx1Cre) using anti–bMunc13-2 and anti-Bassoon antibodies. The low-magnification image of the control brain shows discrete bMunc13-2–positive signals, whose number was reduced in the ELKS1 conditional KO sample. Arrowheads in the high-magnification images indicate bMunc13-2–positive structures. Bars: (low magnification) 50 µm; (high magnification) 5 µm. For images represented as heat maps, quantitative score scales are presented at the bottom left of the respective image. (B) Quantification of the percentages of bMunc13-2–positive puncta among Bassoon-positive puncta in control and ELKS1 conditional KO mouse cortex. Areas for analyses were selected based on the Bassoon signal ($n = 5$ images, Student's t test, ***, $P < 0.001$). (C and D) Frequency distributions of the intensity of bMunc13-2 signals in control mice (ELKS1$^{f/f}$) and ELKS1 conditional KO mice (ELKS1$^{f/f}$;Emx1-

al., 2002). We examined the changes of RRP size and P_{vr} 1.4 s after 10-Hz stimulation trains in Munc13-1/2 DKO neurons rescued with bMunc13-2–EYFP or bMunc13-2(Δ145–187)–EYFP. For this purpose, we estimated RRP sizes by applying the hypertonic sucrose solution before and after 10 Hz stimulation trains. In the augmented state, RRP sizes were increased in both bMunc13-2–EYFP- and bMunc13-2(Δ145–187)–EYFP-expressing cells. However, the RRP size increase was significantly larger in cells expressing bMunc13-2–EYFP (3.2 ± 0.3-fold, $n = 28$, normalized to basal, nonaugmented RRP sizes) than in cells expressing bMunc13-2(Δ145–187)–EYFP (2.2 ± 0.4-fold, $n = 22$, $P < 0.005$; Fig. 4 E). We next assessed P_{vr} changes in the augmented state in a subset of cells. P_{vr} values immediately after the 10-Hz train were increased to similar degrees in cells expressing bMunc13-2–EYFP (3.2 ± 0.3-fold, $n = 12$, normalized to basal, nonaugmented P_{vr} values) or bMunc13-2(Δ145–187)–EYFP (2.9 ± 0.4-fold, $n = 11$, $P > 0.05$; Fig. 4 E). Absolute P_{vr} values in each group were almost identical (9.5% ± 0.7% for bMunc13-2–EYFP, $n = 12$, vs. 9.7% ± 1.4% for bMunc13-2(Δ145–187)–EYFP, $n = 11$; Fig. 4 F).

Our electrophysiological data show that the ELKS1-binding region of bMunc13-2 is a major determinant of its priming function at AZs. The reduced EPSC facilitation and augmentation seen with the ELKS1 binding–deficient bMunc13-2(Δ145–187)–EYFP is likely caused by impaired bMunc13-2(Δ145–187)–EYFP accumulation at AZs and the resulting defect in basal SV priming.

ELKS1 is required for proper AZ recruitment of bMunc13-2

Given the selective interaction and colocalization of bMunc13-2 with ELKS1 (Figs. 2, 3, S1, S2, S3, and S4) and the profound defects in the SV priming activity of bMunc13-2 upon mutation of its ELKS1 binding site (Fig. 4), we next tested whether ELKS1 is required for the AZ recruitment of bMunc13-2. For this purpose, we crossed a newly generated $ELKS1^{f/f}$ mouse line (Liu et al., 2014) with an Emx1-Cre mouse line (Gorski et al., 2002) to examine if ELKS1 elimination affects the AZ localization of bMunc13-2. The number of presynaptic Bassoon-positive compartments exhibiting high levels of bMunc13-2 was reduced in the cortex of $ELKS1^{f/f}$;Emx1-Cre mice as compared with $ELKS1^{f/f}$ controls (Fig. 5, A–D) and the hilus of the dentate gyrus (Fig. 5 E). In principle, this finding could be explained by two scenarios: impaired recruitment of bMunc13-2 to a specific subset of synapses or a general reduction of synaptic bMunc13-2 levels. To distinguish between these possibilities, we examined the distribution of the staining intensities of bMunc13-2 spots in $ELKS1^{f/f}$;Emx1-Cre and $ELKS1^{f/f}$ brains (Fig. 5, C and D). We found that $ELKS1^{f/f}$ control tissue contains a small population of bMunc13-2 spots with high labeling intensity, which are absent in $ELKS1^{f/f}$;Emx1-Cre samples. These results indicate that ELKS1 is necessary for proper AZ recruitment of bMunc13-2 in the intact brain.

Deletion of RIMs leads to increased detergent solubility of Munc13-1, likely because the AZ anchoring of Munc13-1 is perturbed in the absence of RIMs (Andrews-Zwilling et al., 2006; Kaeser et al., 2008). To test if ELKS1 has an analogous function as regards bMunc13-2 solubility, we fractionated Triton X-100 soluble and insoluble fractions of cortical synaptosomes from $ELKS1^{f/f}$;Emx1-Cre mice and $ELKS1^{f/f}$ controls. Using Western blotting, we then determined the distribution of bMunc13-2, which usually partitions predominantly into the insoluble fraction. The insoluble synapse marker PSD95 and the soluble Rab regulator RabGDI (Rab GDP dissociation inhibitor) were used as controls for the insoluble and soluble fractions, respectively. Along with a strong reduction of ELKS1 levels caused by the conditional KO, bMunc13-2 levels in the insoluble synaptosome fraction were significantly reduced in $ELKS1^{f/f}$;Emx1Cre samples as compared with the $ELKS1^{f/f}$ control, whereas bMunc13-2 levels in the soluble fraction or in the homogenate showed no differences between $ELKS1^{f/f}$;Emx1Cre and $ELKS1^{f/f}$ samples (Fig. 6), indicating that the loss of ELKS1 leads to defects in AZ anchoring of bMunc13-2.

These results show that ELKS1 is required for proper AZ targeting and anchoring of bMunc13-2. Hence, the specific interaction of bMunc13-2 with ELKS1 is likely a key determinant of the heterogeneous distribution of bMunc13-2 to distinct synapse subsets of forebrain neurons.

AZ recruitment of bMunc13-2 depends on ELKS1 binding

ELKSs bind to AZ components such as RIM, Bassoon, Piccolo, and α-Liprin, indicating that they may regulate AZ assembly and/or the function of their binding partners. To further examine whether proper AZ recruitment of bMunc13-2 depends on its interaction with ELKS1, EGFP-tagged full-length bMunc13-2 or bMunc13-2(Δ145–187) lacking the ELKS1-binding domain were expressed in Munc13-1/2 DKO neurons using lentiviral expression. Neurons were fixed with PFA and stained with antibodies to GFP, ELKS1, and Bassoon. In mature cultures (16–20 DIV), bMunc13-2–EGFP was accumulated at presynaptic terminals and colocalized with Bassoon whereas bMunc13-2(Δ145–187)–EGFP showed less colocalization with Bassoon (Fig. 7). Interestingly, the colocalization of ELKS1 with Bassoon was also slightly reduced in bMunc13-2(Δ145–187)–EGFP–expressing neurons (Fig. 7 D). Further, analyses of the distributions of labeling intensities of bMunc13-2–EGFP puncta revealed a reduced intensity of EGFP labeling in Bassoon spots in bMunc13-2(Δ145–187)–EGFP-expressing neurons as compared with bMunc13-2–EGFP-expressing neurons (Fig. 7, E–G).

These data show that bMunc13-2 recruitment to and/or anchoring at AZs is regulated by ELKS1. Furthermore, they indicate a certain degree of interdependence between bMunc13-2 and ELKS1 with regard to AZ recruitment.

The presynaptic dwell time of bMunc13-2 is regulated by ELKS1 binding

To further test whether ELKS1 binding regulates bMunc13-2 anchoring at AZs, we used FRAP and investigated the dy-

Cre) as measured in all bMunc13-2 spots (C) and in bMunc13-2 spots colocalized with Bassoon (D). Note that a small population of bMunc13-2 spots with high bMunc13-2 labeling intensity is present in control, but not ELKS1 conditional KO, tissue. $n = 372$ for control mice and $n = 53$ for ELKS1 conditional KO in C; $n = 35$ for control mice and $n = 16$ for ELKS1 conditional KO in D. (E) Immunohistochemical analysis of the hilus of the dentate gyrus of control mice ($ELKS1^{f/f}$) and ELKS1 conditional KO mice ($ELKS1^{f/f}$;Emx1-Cre) with anti–bMunc13-2 (red) and anti-Bassoon (green) antibodies. The low-magnification images of the control brains (insets) show discrete bMunc13-2–positive signals, whose number was reduced in the ELKS1 conditional KO sample. Arrowheads indicate bMunc13-2–positive structures. Bars: (low -magnification, insets) 50 µm; (high magnification) 5 µm. Data are means ± SEM.

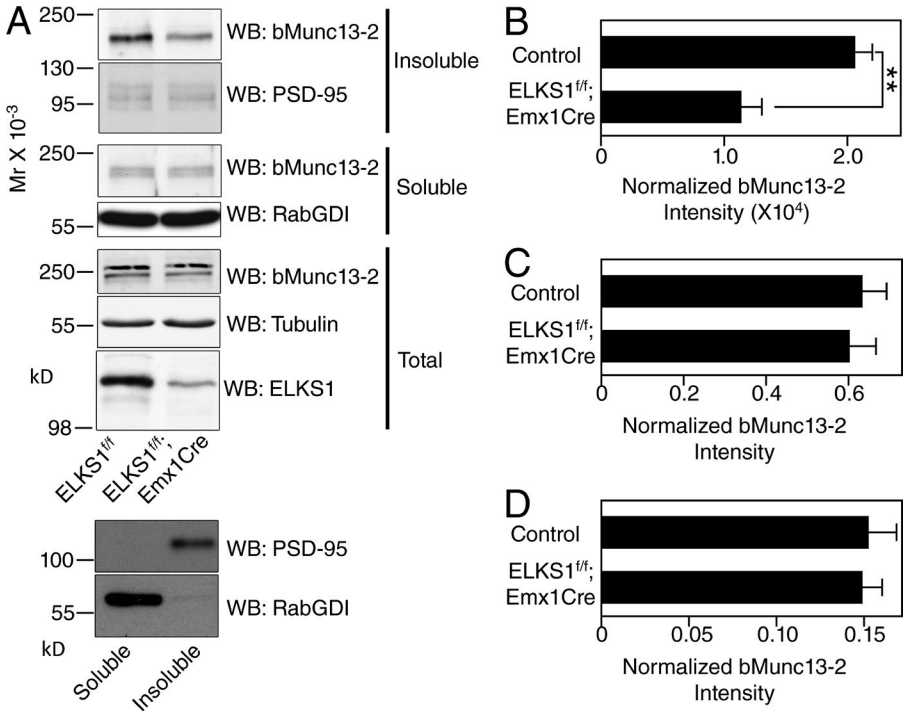

Figure 6. **Partitioning of bMunc13-2 into the insoluble AZ protein fraction depends on the presence of ELKS1.** (A) Western blot (WB) analysis of bMunc13-2 levels in cortex homogenates (total) and in detergent-insoluble and detergent-soluble fractions of cortex synaptosomes from ELKS1$^{f/f}$ and ELKS1$^{f/f}$;Emx-1Cre mice. The two panels at the very bottom show that PSD95 was enriched and RabGDI was depleted in the insoluble fraction. Note that different batches of prestained molecular weight markers were used for the blot sections at the bottom of the top panel (total) so that the molecular weight marker for 250 kD runs at a slightly smaller apparent molecular weight. Further, the soluble bMunc13-2 fraction (third and fifth blot sections from top) typically appears as two bands, both of which are absent in Munc13-2 KO samples. (B–D) Quantification of bMunc13-2 signals in detergent-insoluble (B) and soluble (C) fractions of synaptosomes and in homogenate (D). Band intensities were determined densitometrically on films using ImageJ (soluble and insoluble fractions) or by using Odyssey imaging of blots after incubation with fluorescent secondary antibodies (LICOR). The signals were then normalized to the ones obtained with anti-PSD95 (for B), anti-RabGDI (for C), and antitubulin (for D) antibodies. n = 5 for control and n = 3 for ELKS$^{f/f}$;Emx1-Cre mice for B and C; n = 4 for control and for ELKS$^{f/f}$;Emx1-Cre mice for D; Student's t test, **, P < 0.01 for B, P = 0.756 for C, and P = 0.90 for D. Data are means ± SEM.

namics of bMunc13-2 localization in presynapses. When bMunc13-2–EGFP or ELKS1 binding–deficient bMunc13-2(Δ145–187)–EGFP were expressed in mature mouse hippocampal Munc13-1/2 DKO neurons (16–20 DIV) using a calcium phosphate transfection, EGFP signals were often distributed diffusely along axons (unpublished data), indicating that the overexpressed bMunc13-2 proteins had saturated the endogenous AZ anchoring machinery.

To circumvent this, we additionally overexpressed recombinant ELKS1 containing a nested tdTomato sequence (tdTom-ELKS1). When corresponding neurons were fixed and stained for Bassoon, most puncta positive for both tdTomato and bMunc13-2–EGFP partially colocalized with endogenous Bassoon, whereas puncta positive for only EGFP did not, indicating that overexpressed tdTom-ELKS1 recruits recombinant bMunc13-2–EGFP to the presynapse (Fig. 8 A). Interestingly, bMunc13-2(Δ145–187)–EGFP was also enriched at the Bassoon-positive puncta when coexpressed with tdTom-ELKS1 (Fig. 8 A), indicating that excess ELKS1 has the potential to recruit bMunc13-2 to AZs via alternative pathways.

For FRAP experiments, synaptic fluorescence of bMunc13-2–EGFP or bMunc13-2(Δ145–187)–EGFP colocalized with tdTom-ELKS1 was bleached rapidly with high-intensity laser illumination, and FRAP at bleached synapses was examined using time-lapse confocal microscopy to infer bMunc13-2 dwell times (Fig. 8, B and C). Puncta of bMunc13-2–EGFP at bleached synapses recovered gradually in two phases (Fig. 8, C–E), each of which contributed ∼50% of the total FRAP (τ_1 = 2.75 min, 42%; τ_2 = 57.9 min, 58%; n = 31 synapses, nine cells). These data indicate the presence of two different bMunc13-2 pools at AZs. Both pools recover gradually after photobleaching, indicating that bMunc13-2 is not recruited to AZs in discrete transport packages, as may occur during neuronal differentiation (Shapira et al., 2003). Because the time constant of free passive diffusion is ∼1 s, the fast phase of bMunc13-2–EGFP FRAP likely reflects a soluble pool of bMunc13-2–EGFP that enters the synaptic terminal by "buffered" diffusion and that associates with low-affinity binding sites. In contrast, the slowly recovering pool likely represents bMunc13-2–EGFP that is anchored and partially immobilized at the AZ. Although WT bMunc13-2–EGFP showed a FRAP with two phases of equal weight, the major fraction of ELKS1-binding–deficient bMunc13-2(Δ145–187)–EGFP at synaptic terminals recovered within the fast FRAP phase, whose time constant was very similar to that seen with bMunc13-2–EGFP (τ_1 = 2.74 min, 73%; τ_2 = 24.6 min, 27%; n = 31 synapses, seven cells; Fig. 8 E).

Our FRAP data show that the N-terminal ELKS1-binding region of bMunc13-2 is a critical determinant of bMunc13-2 mobility at AZs, further supporting the notion that proper AZ anchoring of bMunc13-2 depends on ELKS1 binding. Accordingly, further analyses showed that FRAP of bMunc13-2–EGFP at synapses containing high tdTom-ELKS1 levels is slower and less pronounced than at synapses with low tdTom-ELKS1 levels (Fig. 9).

Discussion

Evolution of AZ anchoring domains in Munc13s

Presynaptic AZs are late evolutionary acquisitions, and the currently known AZ proteins are not expressed in plants or fungi and rarely found in nonneuronal tissues. As members of the Munc13 family of SV priming proteins at AZs are essential for SV exocytosis (Augustin et al., 1999b; Varoqueaux et

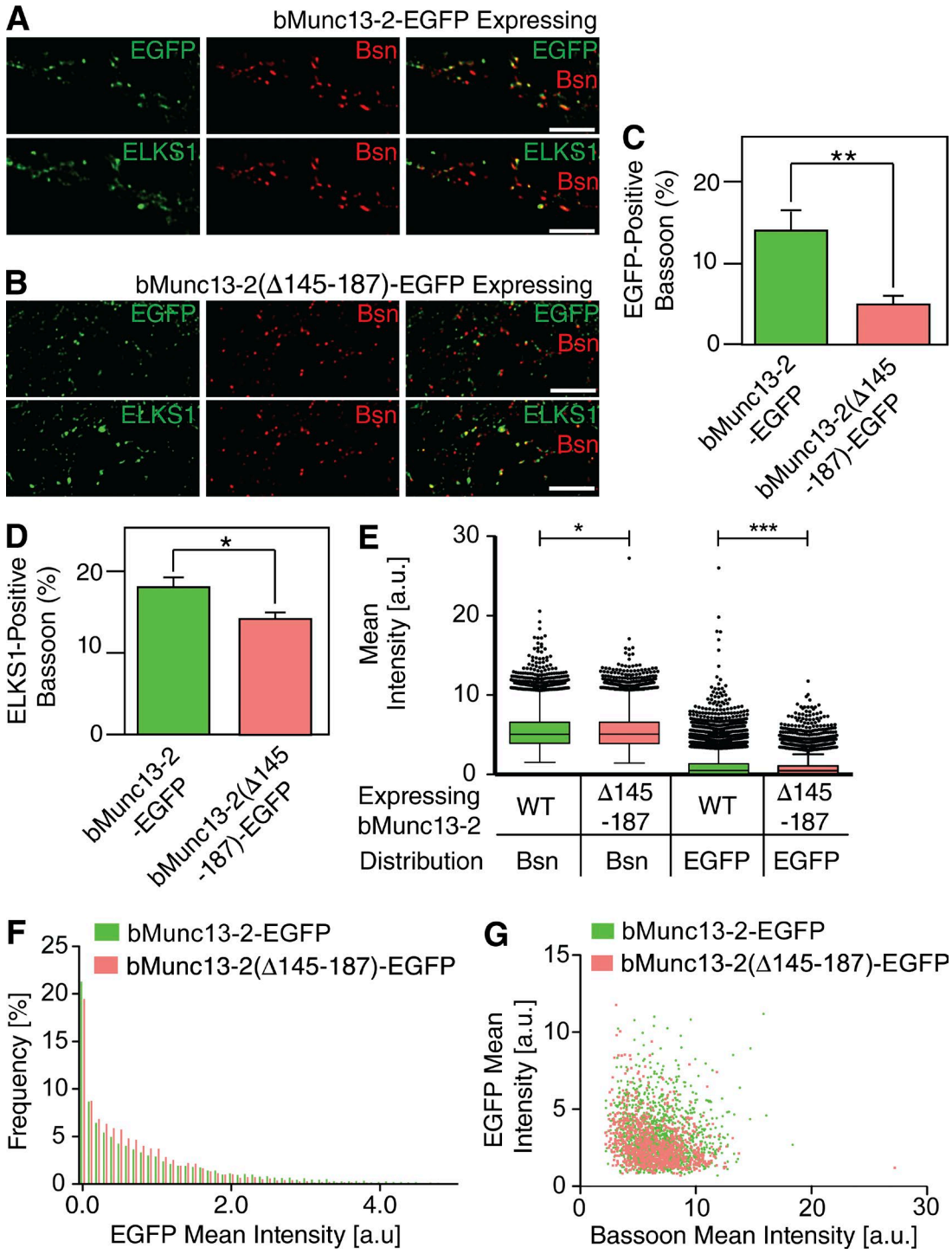

Figure 7. **ELKS binding regulates the recruitment of bMunc13-2 to AZs in cultured hippocampal neurons.** (A and B) Munc13-1/2 DKO neurons expressing the indicated bMunc13-2–EGFP fusion constructs. Neurons were costained for GFP, ELKS1, and Bassoon. bMunc13-2–EGFP expressed in Munc13-1/2 DKO neurons formed punctate structures and colocalized with immunostained Bassoon (A), whereas bMunc13-2(Δ145–187)–EGFP puncta showed only partial colocalization with Bassoon (B). Note that ELKS1 showed colocalization with Bassoon in A and B. Bars, 5 µm. (C and D) Quantification of the fractions of EGFP-positive (C) and ELKS1-positive (D) Bassoon spots in neurons expressing bMunc13-2–EGFP or bMunc13-2(Δ145–187)–EGFP. $n >$ 25,000 spots were analyzed for EGFP, ELKS1, or Bassoon. Student's *t* test (**, $P < 0.01$; *, $0.01 < P < 0.05$). (E) Tukey box and whisker plot for mean intensities of EGFP and Bassoon signals (Bsn) in Bassoon spots of cultured neurons expressing bMunc13-2–EGFP (green) or bMunc13-2(Δ145–187)–EGFP (red). Boxes represent values from upper and lower quartiles, horizontal lines represent medians, vertical lines cover 99% of all values, and outliers are represented as filled circles. Bassoon puncta intensities show a slight reduction in bMunc13-2(Δ145–187)–EGFP-expressing neurons as compared with Munc13-2–EGFP-expressing neurons (5.441 ± 0.016, n = 16,850 in Munc13-2–EGFP-expressing neurons; 5.391 ± 0.015, n = 18,208 in Munc13-2(Δ145–187)–EGFP-expressing neurons; *, $P = 0.0173$). EGFP signals show a stronger intensity reduction in bMunc13-2(Δ145–187)–EGFP-expressing neurons than Munc13-2–EGFP-expressing neurons (0.991 ± 0.010, n = 16,850 in Munc13-2–EGFP-expressing neurons; 0.770 ± 0.007, n = 18,208 in Munc13-2(Δ145–187)–EGFP-expressing neurons; ***, $P < 0.001$). (F) Frequency distributions of EGFP signal intensities in Bassoon spots in bMunc13-2–EGFP- (green) or bMunc13-2(Δ145–187)–EGFP-expressing (red) neurons. Note that bMunc13-2–EGFP-expressing neurons have a small fraction of Bas-

al., 2002), their specific localization at AZs (Figs. 1, 3, 5, 7, 8, 9, S2, S3, and S4; Betz et al., 1998; Rhee et al., 2002) is a key determinant of the AZ restriction, speed, and efficacy of neurotransmitter release.

The present data show that during evolution, different Munc13s acquired different mechanisms for their specific AZ targeting and anchoring. The C-terminal two thirds of all mammalian Munc13 sequences, the R modules, are conserved from *Drosophila* (Unc13) and *C. elegans* (Unc-13). They contain a C_1 domain, a C_2 domain (C_2B), two Munc13 homology domains, and a C-terminal second C_2 domain (C_2C; Koch et al., 2000). In *C. elegans*, the Unc-13 R module is associated with one of two types of N termini, the M module or the L module (Kohn et al., 2000). Although the M module represents a unique sequence that is not found in mammalian Munc13s, the L module is homologous to the N termini of Munc13-1 and ubMunc13-2. These contain another C_2 domain (C_2A) and a Ca^{2+}/CaM-binding motif, which determine RIM-dependent AZ recruitment and regulation, fast neurotransmitter release, and Ca^{2+}/CaM-dependent short-term plasticity in *C. elegans* and mammals (Betz et al., 2001; Junge et al., 2004; Andrews-Zwilling et al., 2006; Deng et al., 2011; Kaeser et al., 2011; Hu et al., 2013). Thus, the LR-form of Unc-13 has been under strong evolutionary selection pressure, whereas the M module was lost during evolution, likely because it is neither selectively targeted to nor anchored at AZs (Nurrish et al., 1999).

The organization of the mammalian Munc13-2 gene is similar to that of *C. elegans unc-13*. Two promoters drive the expression of a widely expressed ubMunc13-2 variant and a largely brain-specific bMunc13-2 variant. The ubMunc13-2 N terminus is homologous to the Unc-13 L module and to the N terminus of Munc13-1, whereas bMunc13-2 contains a novel N terminus instead of the L module. The two different Munc13-2 N termini are spliced into a common C-terminal sequence, which is similar in all Munc13s. Like bMunc13-2, Munc13-3 contains a novel N terminus that is different from all other Munc13 sequences apart from a short coiled-coil motif that is 52% identical to the ELKS1-binding motif in bMunc13-2 and conserved at least from fish to *Homo sapiens*. We show here that stoichiometric binding of this motif to ELKS1 (Fig. 2) mediates a novel ELKS1-dependent AZ targeting process for bMunc13-2, but not for Munc13-3, which does not bind ELKS1.

It thus seems that in the case of the bMunc13-2 N terminus, parallel evolution created a sequence motif that allows for a novel AZ anchoring mechanism via ELKS1 binding, which is analogous to the RIM-mediated mechanism that anchors ubMunc13-2 and Munc13-1 to AZs and regulates their activities (Betz et al., 2001; Junge et al., 2004; Andrews-Zwilling et al., 2006; Deng et al., 2011). In this regard, the type of bMunc13-2-ELKS1 interaction described in the present study appears to be a more recent evolutionary acquisition, whereas the interaction between Munc13-1 or ubMunc13-2 and RIMs is phylogenetically older. This notion is supported by genetic studies in *C. elegans*, which showed that Unc-13 and Unc-10 (RIM), but not Unc-13 and ELKS, act in the same SV priming pathway (Koushika et al., 2001; Deken et al., 2005).

The evolutionary selection pressure to conserve AZ anchoring of Munc13-like proteins and a striking parallelity of corresponding selection processes are also evident with regard to *Drosophila* Munc13 proteins. As is the case for *C. elegans* Unc-13 and mammalian Munc13-2, the *Drosophila unc-13* locus generates two Unc13 variants, Unc13A and Unc13B, with identical R modules but different N termini, which result from the alternative use of two large exons. Fascinatingly, the N termini of *Drosophila* Unc13A and Unc13B are not related to those of mammalian bMunc13-2 and ubMunc13-2 (or of *C. elegans* Unc-13 MR and Unc-13-LR). Nevertheless, Brp, the *Drosophila* homologue of ELKSs, binds directly to the Unc13A N terminus and recruits Unc13A to AZs, although this interaction involves an N-terminal region of Brp that is not related to the ELKS1 region that we identified as the bMunc13-2 interaction domain. In other words, evolution created an AZ recruitment mechanism in *Drosophila* that functionally resembles the bMunc13-2 interaction with ELKS1 described in the present study and even involves the same protein types but uses completely different primary sequences and hence a different binding mechanism (Böhme et al., 2016).

Differential AZ targeting of Munc13s and synapse heterogeneity

Hippocampal neurons express Munc13-1 and bMunc13-2, and synapses of such neurons exhibit synaptic depression if they contain Munc13-1, whereas frequency facilitation and augmentation characterize synapses containing bMunc13-2 (Fig. 4; Rosenmund et al., 2002). Interestingly, individual cultured hippocampal neurons equip the majority of their synapses with Munc13-1 alone and only a subset of synapses with Munc13-1 and bMunc13-2 (Fig. 1). Likewise, only a small subset of synapses in hippocampus and cortex recruit bMunc13-2 (Figs. 3 and S3). Such differential distribution of Munc13s may determine the synaptic output mode of neurons in a synapse-specific manner by conveying different short-term synaptic plasticity characteristics and may thus directly affect neuronal network function.

We discovered a mechanism by which synapses can be equipped with either Munc13-1 alone or with Munc13-1 and bMunc13-2. According to our earlier findings, Munc13-1 recruitment to and anchoring at AZs depends on RIMs (Andrews-Zwilling et al., 2006). Instead, AZ recruitment and anchoring of bMunc13-2 requires ELKS1 (Figs. 5 and 6), so that bMunc13-2 accumulates at a subset of synapses that are distinctly enriched in ELKS1 (Figs. 3 and S3), but not at the many other synapses with lower ELKS1 levels. The upstream processes that lead to the particular enrichment of ELKS1 at defined subsets of synapses remain unknown but likely involve extracellular and trans-synaptic signaling, such as via cell adhesion proteins (Takahashi et al., 2011).

Different axon terminals of one and the same neuron can exhibit different forms of short-term plasticity (e.g., depending on the target cell they contact within a neuronal network; Reyes et al., 1998). Such synapse-specific differences in short-term plasticity can in principle have multiple

soon spots with high EGFP intensity. *n* = 16,850 for bMunc13-2–EGFP-expressing neurons and *n* = 18,208 for bMunc13-2(Δ145–187)–EGFP-expressing (red) neurons. (G) Scatterplots showing relationships between mean intensities of EGFP and Bassoon signals in bMunc13-2–EGFP- (green) or bMunc13-2(Δ145–187)–EGFP-expressing (red) neurons. Mean intensities were quantified from Bassoon and EGFP colocalizing spots. *n* = 1,549 for bMunc13-2–EGFP-expressing neurons and *n* = 895 for bMunc13-2(Δ145–187)–EGFP-expressing (red) neurons. Data are means ± SEM.

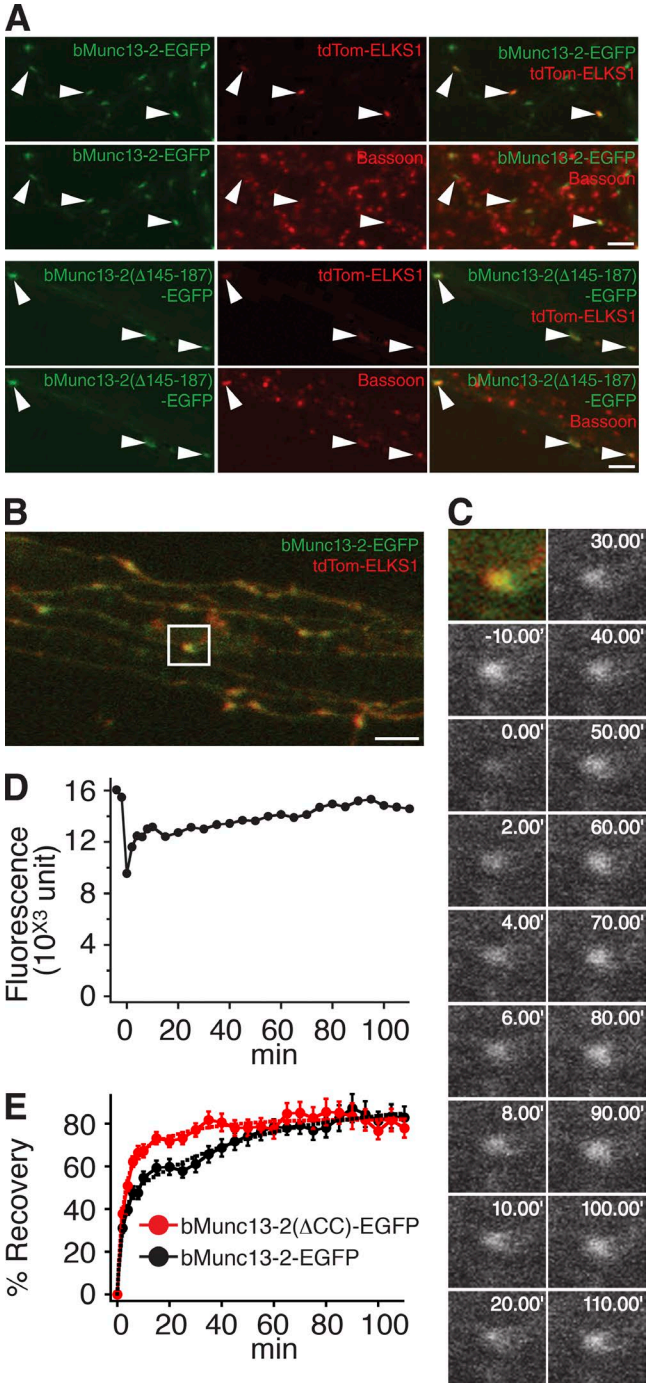

Figure 8. **ELKS binding anchors bMunc13-2 to AZs in cultured hippocampal neurons.** (A) Representative three-channel images of neurons expressing bMunc13-2–EGFP (top two rows) or bMunc13-2(Δ145–187)–EGFP (bottom two rows) together with tdTom-ELKS1. Neurons were fixed and stained with an anti-Bassoon antibody. Note that most of the recombinant bMunc13-2 signals colocalizing with tdTom-ELKS1 were accumulated at Bassoon-positive AZs (arrowheads). Bars, 5 µm. (B) Overview of axonal terminals imaged in the FRAP experiment in C. The region of interest for the FRAP experiment is indicated by the white box. Bar, 5 µm. (C) Images of a representative FRAP experiment with bMunc13-2–EGFP in Munc13-1/2 DKO neurons. The synapse was bleached, and images were obtained at 2-min intervals for the first 10 min after bleaching and subsequently at 5-min intervals. Images are shown at 10-min intervals after the first 10 min. (D) Time course of FRAP at the synapse shown in C. (E) Mean FRAP time course of the indicated bMunc13-2–EGFP constructs at synapses in Munc13-1/2 DKO neurons. The fluorescence recovery of bMunc13-2(Δ145–187)–EGFP was faster as compared with that of bMunc13-2–EGFP. Solid lines are mean traces measured for the two constructs. Dashed lines are results of fitting with two exponential curves. Data for bMunc13-2–EGFP are from 31 synapses (nine cells), and data for bMunc13-2(Δ145–187)–EGFP are from 31 synapses (seven cells). Data are means ± SEM.

molecular causes, ranging from differences in the type or abundance of presynaptic voltage-gated ion channels to heterogeneities in the composition of the SV priming and release machinery, including Munc13s (Bao et al., 2010). However, how such molecular and functional differences are generated at the level of individual presynapses is unknown. Based on the data presented here, we propose that the ELKS1–bMunc13-2 interaction is a core component of a novel molecular mechanism by which differences in presynaptic function can be brought about.

Turnover of AZ proteins

We used a FRAP approach to study the turnover of bMunc13-2 and bMunc13-2(Δ145–187) at AZs. For optimal performance of the assay, we had to coexpress tdTom-ELKS1 along with the bMunc13-2 variants. Although this is a caveat that has to be considered in certain contexts (e.g., regarding absolute AZ dwell times), our approach reliably detected differences in AZ dwell times between bMunc13-2 and its ELKS1-binding–deficient mutant. Our FRAP data indicate that the residence time of bMunc13-2 at AZs is rather short (τ = 57.9 min; Fig. 8). Similar turnover rates were observed for the *Drosophila* Munc13 homologue Dunc-13 at neuromuscular synapses (Aravamudan and Broadie, 2003; Speese et al., 2003) and for mammalian Munc13-1 (Kalla et al., 2006). The AZ dwell time of bMunc13-2 is dependent on ELKS1 binding and reduced if this interaction is perturbed (Fig. 8) or synaptic ELKS1 levels are low (Fig. 9). This indicates that ELKS1, which interacts directly or indirectly with almost all other known AZ proteins and plays a key role in AZ function (Liu et al., 2014; Held et al., 2016), physically anchors bMunc13-2 at AZs. It thus appears that the proteinaceous cytomatrix at AZs is created by protein–protein interactions of substantial affinity, which are still readily reversible in some cases. The high turnover rate of Munc13s at AZs may represent an important basis for the fast and reversible adjustment of transmitter release efficacy and synaptic strength.

Functional relevance of AZ targeting and anchoring of Munc13s

The present study shows that the perturbation of ELKS1 binding to bMunc13-2 has substantial consequences. First, ELKS1 binding–deficient bMunc13-2 is not properly targeted to AZs (Fig. 7). Second, endogenous bMunc13-2 is not properly recruited to AZs if ELKS1 is genetically eliminated (Figs. 5 and 6). Third, the synaptic turnover rate of bMunc13-2 is inversely correlated to synaptic ELKS1 levels (Fig. 9), and the synaptic turnover rate of ELKS1 binding–deficient bMunc13-2(Δ145–187) is faster than that of WT bMunc13-2 (Fig. 8). Fourth, even when overexpressed at very high levels, ELKS1 binding–deficient bMunc13-2(Δ145–187) fails to functionally rescue transmitter release in Munc13-1/2 DKO neurons in many of the cells tested (Figs. 4 and S5). Fifth, even upon successful rescue of transmitter release in Munc13-1/2 DKO neurons, expression of ELKS1 binding–deficient bMunc13-2(Δ145–187) leads to aberrant SV priming and changes in synaptic short-term plasticity (Figs. 4 and S5).

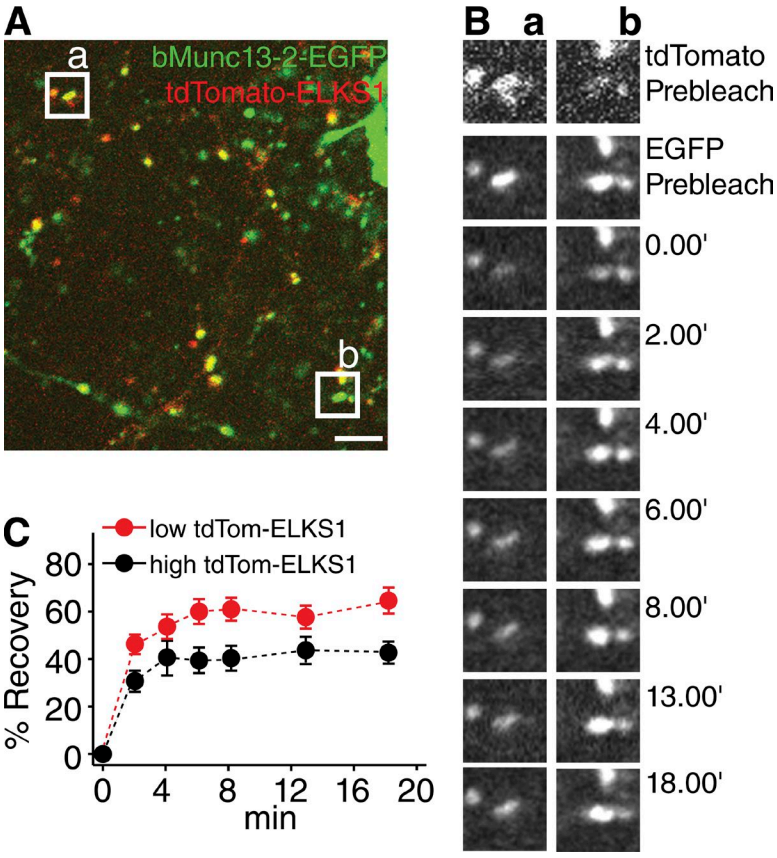

Figure 9. **Turnover of bMunc13-2 at AZs depends on ELKS1 levels.** (A) Overview of axonal terminals imaged in the FRAP experiment in B. The regions of interest for the FRAP experiment are indicated by white boxes (a and b). Bar, 5 µm. (B) Representative images of tdTom-ELKS1 (top) and bMunc13-2–EGFP (second panels from top) before bleaching and recovery of EGFP signals along the time course at synapses with high (a) or low (b) tdTom-ELKS1 levels. (C) Mean FRAP time courses of bMunc13-2–EGFP at synapses with high (black, n = 22) or low (red, n = 22) levels of tdTom-ELKS1. Note the more rapid recovery of bMunc13-2–EGFP at synapses with low levels of tdTom-ELKS1 in B and C. Data are means ± SEM.

Although it is possible that additional interactions of bMunc13-2 with AZ proteins, involving regions outside the ELKS1 binding motif described in the present study (i.e., residues 145–187 of bMunc13-2), contribute to the AZ recruitment of bMunc13-2 (Fig. 8 A), our data show that (a) AZ accumulation and anchoring of bMunc13-2 has to surpass a critical threshold level to allow for efficient SV priming to occur and that (b) the bMunc13-2–ELKS1 interaction described here plays a substantial role in this AZ accumulation process. Further, the reduced evoked EPSC amplitudes, RRP, facilitation, and augmentation observed in Munc13-1/2 DKO neurons expressing bMunc13-2(Δ145–187) despite very high expression levels (Figs. 4 and S5) show that the mere presence of bMunc13-2 in the proximity of AZs is not sufficient to reconstitute full functionality. Rather, bMunc13-2 has to be functionally integrated into the AZ scaffold, and its absolute levels within AZs determine basal priming activity and, consequently, short-term plasticity.

As far as AZ recruitment and ultimate functional consequences are concerned, the ELKS1–bMunc13-2 interaction described here is analogous to the RIM–Munc13-1 and RIM–ubMunc13-2 interactions (Betz et al., 2001; Andrews-Zwilling et al., 2006). RIM binding–deficient variants of Munc13-1 either do not or only partially rescue the priming deficit in Munc13-1 KO neurons (Betz et al., 2001), and in RIM1α KO, RIM1/2 DKO, and Munc13-1 KO neurons, short-term plasticity characteristics are changed from a mainly depressing to a partly facilitating and augmenting phenotype (Rosenmund et al., 2002; Calakos et al., 2004; Deng et al., 2011; Kaeser et al., 2011). As with bMunc13-2, these observations indicate that the presynaptic levels of Munc13-1 have to pass a certain threshold level and that Munc13-1 has to be integrated into the AZ protein network for proper function. Importantly, though, RIMs regulate the function of Munc13-1 and ubMunc13-2 beyond AZ recruitment and anchoring by reversing the autoinhibitory homodimerization of Munc13-1 and ubMunc13-2, which is mediated by the N termini of the respective Munc13s (Dulubova et al., 2005; Deng et al., 2011). It is unlikely that ELKS1 exerts a similar effect on bMunc13-2, because the dimerization motif of Munc13-1 and ubMunc13-2 is not conserved in bMunc13-2.

Consistent with the data presented here, cultured hippocampal neurons of ELKS1/2 DKO exhibit diverse effects on SV priming. Whereas excitatory hippocampal neurons show a 40% reduction in RRP size upon ELKS1/2 DKO (Held et al., 2016), no RRP deficit is observed at inhibitory synapses in the same mutants (Liu et al., 2014). Our current dataset indicates a role of the ELKS1–bMunc13-2 interaction in SV priming but does not explain all effects of ELKSs in SV priming. Complete loss of Munc13-2 from cultured GABAergic or glutamatergic hippocampal neurons does not cause changes in SV priming because Munc13-1 function dominates in these neurons (Varoqueaux et al., 2002). Instead, Munc13-2 loss causes functional changes in synaptic efficacy and plasticity only in defined microcircuits and subsets of synapses in situ, such as in the CA3 region of the hippocampus (Breustedt et al., 2010). It is therefore not unexpected that aberrant recruitment of bMunc13-2 in the absence of ELKS1 as shown in the present study (Figs. 5 and 6) does not lead to substantial changes in overall SV priming and that the consequences of ELKS1 deletion for bMunc13-2 localization and function can only be seen if detailed and synapse-specific analyses are performed (Figs. 5 and 6), if bMunc13-2 is studied in isolation (i.e., in the absence of other Munc13s; Figs. 4 and S5), or if defined microcircuits and subsets of synapses are examined (Breustedt et al., 2010). In addition, it is possible that the present and previous studies have partly underestimated the

relevance of ELKS C-terminal sequences for synaptic transmission, because both ELKS genes contain sequences that express β isoforms containing these C-terminal sequences at low abundance (Kaeser et al., 2009; Liu et al., 2014) and that are not removed in our ELKS1 and ELKS2 KO mice.

In any case, further studies on the functional role of the ELKS1–bMunc13-2 interaction in the brain will require detailed analyses of specific synaptic contacts and microcircuits in ELKS1 or bMunc13-2 KO mice to show which synaptic signaling processes depend upon the proper AZ recruitment of bMunc13-2 by ELKS1 and which of the many examples of presynaptic functional heterogeneity, particularly regarding short-term plasticity, depend upon the ELKS1–bMunc13-2 interaction.

Materials and methods

Antibodies

A polyclonal guinea pig anti–bMunc13-2 antibody was generated using GST-fused rat bMunc13-2(1–305) (GenBank accession no. NM_022862) as the antigen. Anti-ELKS1 and anti-ELKS2 rabbit polyclonal antibodies were raised against GST-fused rat ELKS1(73–185) (GenBank accession no. NM_170788.2) and rat ELKS2(63–181) (GenBank accession no. NM_170787.1), respectively. Antibodies were affinity purified from the respective antisera using antigen proteins coupled to HiTrap NHS-activated HP columns (GE Healthcare). Mouse monoclonal (clone SAP7F407) anti-Bassoon antibody was from Enzo Life Sciences. Guinea pig polyclonal anti-Bassoon and anti–Munc13-1 antibodies were from Synaptic Systems. Rabbit polyclonal and mouse monoclonal anti-GFP (clone 3E6) antibodies were from MBL and Molecular Probes, respectively.

Mouse lines

Munc13-1 and Munc13-2 KOs (Augustin et al., 1999b; Varoqueaux et al., 2002), ELKS2 KOs (Kaeser et al., 2009), the Emx1Cre mouse line (Gorski et al., 2002), and the ELKS1$^{f/f}$ mouse line (Liu et al., 2014) were published previously.

Immunocytochemistry and immunohistochemistry

Primary hippocampal neurons in autaptic culture were prepared from Munc13-2^{EYFP} KI mice (Cooper et al., 2012), We used a modified version of the microisland culture system (Burgalossi et al., 2012), where astrocytes were cultured on a separate coverslip to allow for medium conditioning while avoiding immunostaining background contributed by astrocytes. First, dissociated neurons were plated on 6-well plates with 32-mm-diameter glass coverslips that had been coated with poly-L-lysine using a stamp with an array of 400 µm × 400 µm microsquares. 2–3 d later, ∼200-mm^2 coverslip fragments with cultured astrocytes were placed into the same wells with the neuron cultures. Autaptic neurons were fixed with 4% paraformaldehyde in PBS and immunostained with a rabbit polyclonal anti-GFP antibody, a guinea pig polyclonal anti–Munc13-1 antibody, and a mouse monoclonal anti-Bassoon antibody for staining of Munc13-2–EYFP, Munc13-1, and Bassoon. Autaptic neurons were stained with a rabbit polyclonal anti-ELKS1 antibody, a guinea pig polyclonal anti-Munc13-1 antibody, and a mouse monoclonal anti-Bassoon antibody for staining of ELKS1, Munc13-1, and Bassoon. Primary cultured Munc13-1/2 DKO neurons expressing bMunc13-2–EGFP (Banker and Cowan, 1977) were fixed with cold methanol (−20°C) and immunostained with a mouse monoclonal anti-GFP antibody and a guinea pig anti-Bassoon antibody to label AZs, or with a rabbit anti-ELKS1 antibody. Primary cultured Munc13-1/2 DKO neurons expressing bMunc13-2–EGFP and tdTom-ELKS1 (Banker and Cowan, 1977) were fixed with 4% paraformaldehyde in PBS and immunostained with a mouse monoclonal anti-Bassoon antibody. Tissue sections prepared from control, Munc13-2 KO (Varoqueaux et al., 2002), ELKS2 KO (Kaeser et al., 2009), and ELKS1$^{f/f}$;Emx1-Cre (Gorski et al., 2002; Liu et al., 2014) mice were fixed with cold methanol (−20°C) and immunostained with anti-ELKS1, anti-ELKS2, or anti-bMunc13-2 antibodies, together with a mouse monoclonal anti-Bassoon antibody (Stressgene).

YTH screens and binding assays

YTH vectors encoding the GBD in frame with the proteins of interest were constructed in pGBDC2. A YTH screen using a mouse embryo cDNA prey library in a modified pGAD vector, which encodes GAD fusion proteins, and pGBDC2-bMunc13-2(1–605), which encodes GBD-bMunc13-2(1–605), as bait were performed as described previously (James et al., 1996). Binding regions were mapped using pGBDC2-based bait vectors encoding corresponding fragments of bMunc13-2 or Munc13-3 (GenBank accession no. NM_173146) and pGAD-ELKS1(771–976) as prey.

Expression vectors and protein expression

Bacterial expression vectors encoding GST and MBP in frame with various sequences of ELKSs and bMunc13-2 were constructed in pGEX-4T-1 (GE Healthcare) or pMalC2 (New England Biolabs, Inc.). Recombinant proteins were expressed in and purified from *Escherichia coli* strain BL21DE3 using glutathione–Sepharose 4B (GE Healthcare) or amylose resin (New England Biolabs, Inc.). Lentivirus expression vectors encoding bMunc13-2 variants in frame with a C-terminal EGFP tag were constructed in a modified FUGW vector containing a synapsin promoter instead of a ubiquitin promoter (Lois et al., 2002). The lentiviral construction vectors pMD2.G and pCMVΔR8.2 were gifts from D. Trono (École Polytechnique Fédérale de Lausanne, Lausanne, Swizerland; Follenzi and Naldini, 2002; Barde et al., 2010; Hsia et al., 2014). Semliki Forest virus expression vectors encoding bMunc13-2 variants in frame with a C-terminal EGFP tag were constructed in pSCA1 (DiCiommo and Bremner, 1998). Mammalian expression vectors encoding bMunc13-2 variants with EGFP or EYFP sequences attached at their C termini were constructed in pEGFP-N1 or pEYFP-N1 (BD) as described previously (Betz et al., 1998), and vectors encoding bMunc13-2 and ELKS variants with EGFP, ECFP, or EYFP attached at their N termini were constructed in pEGFP-C2, pECFP-C1, or pEYFP-C1 (BD). A mammalian expression vector encoding rat ELKS1 (Wang et al., 2002) with a nested tdTomato sequence between residues 140 and 141 (. . . SMASTVP-dtTomato-HSLRQ . . .) of ELKS1 was constructed in pCMV5. Primary cultures of hippocampal neurons were prepared and transfected using the calcium phosphate method (Dresbach et al., 2003) or infected with lentivirus (Follenzi and Naldini, 2002; Barde et al., 2010) to express recombinant proteins and used for immunocytochemistry.

Biochemical assays

For GST cosedimentation assays, 20 or 70 µg purified MBP-bMunc13-2(1–305) was incubated with 20 µg GST-ELKS1(771–976) (GenBank accession no. AF340028) or GST-ELKS2(751–969) (GenBank accession no. AY356530) immobilized on 50 µl glutathione–Sepharose 4B beads for 14 h at 4°C in A-buffer (20 mM Tris/HCl, pH 7.5, 1 mM EDTA, 1 mM DTT, 150 mM NaCl, 0.2 mM PMSF, 1 µg/ml aprotinin, and 0.5 µg/ml leupeptin) containing 0.1% Triton X-100 (Roche). Beads were then washed with the same buffer, and bound proteins were analyzed by SDS-PAGE and Coomassie Brilliant blue staining. For

immunoprecipitations, synaptosomes prepared from Munc13-2^{EYFP} KI mouse hippocampi were solubilized at protein concentrations of 3 mg/ml in A buffer containing 0.8% sodium cholate (Wako Pure Chemical Industries) and incubated on ice for 30 min. After diluting the sample with the same volume of A-buffer containing 1% Triton X-100, all subsequent procedures were performed as described previously (Betz et al., 1998) using antibodies to GFP (Abcam).

FRET and FRAP analyses

For FRET analysis, primary rat hippocampal neurons were transfected with plasmids encoding ECFP-bMunc13-2(70–204) and EYFP-ELKS1(771–976) or with the positive control construct pECFP-15AA-EYFP encoding an ECFP–EYFP fusion protein with a 15-residue linker. Cells coexpressing ECFP and EYFP were used as a negative control. After expression for 96 h, FRET measurements were performed as described previously (Neculai et al., 2005). For FRAP imaging experiments shown in Fig. 8, neurons were cultured on a glass-bottom culture dish (ibidi) and incubated in a Hepes-buffered growth medium, pH 7.4, without perfusion. Neurons were observed using a confocal laser scanning microscope (ZEISS LSM 510 Meta) with a 40× oil-immersion objective lens (numerical aperture, 1.3). The system was controlled by ZEISS Zen software combined with the Multiple Time Series macro (ZEISS). The temperature of the culture dish and objective lens were adjusted to 37°C by Tempcontrol 37–2 digital (ZEISS). An argon laser was used to excite EGFP at 488 nm, and a long-pass 505-nm filter was used to read the fluorescence emissions. To correct focal drift during imaging, we used the autofocus macro of the ZEISS LSM software and averaged seven frames scanned at seven different focal planes spaced at 1.0-µm intervals. Images were collected at 512 × 512–pixel resolution (pixel size, 0.22 × 0.22 µm). Synaptic fluorescence of bMunc13-2–EGFP or bMunc13-2(Δ145–187)–EGFP colocalized with tdTom-ELKS1 was imaged in live neurons. EGFP puncta colocalizing with tdTomato signals were bleached. Photobleaching was achieved by transiently increasing the excitation power to 30–50%, scanning only the synaptic boutons of interest 50 times (total of 160 µs per pixel). For FRAP experiments shown in Fig. 9, neurons on a glass-bottom culture dish (ibidi) in the growth medium were monitored with a Nikon Eclipse Ti microscope equipped with hardware autofocus (Perfect Focus), a spinning-disk confocal unit (W1; Yokogawa Electric Corporation), and an Andor FRAPPA unit used for bleaching. During imaging, the humidity, temperature, and CO_2 concentration of the culture were maintained at 95–98%, 37°C, and 5%, respectively. Fluorescence generated by transduced neurons was observed with a 100× oil-immersion objective lens (numerical aperture 1.49) upon 488-nm and 561-nm sequential laser excitation for the EGFP and tdTomato fluorophores, respectively. Z-drift was automatically compensated during the acquisition of 1,024 × 1,024–pixel images (pixel size, 0.129 × 0.129 µm). XY-drift was compensated with NIS Elements version 4.50. The intensity of tdTomato relative to prebleaching EGFP was estimated from 148 bleached synapses. FRAP of EGFP from synapses representing the top and bottom 15% of the relative tdTomato intensities ($n = 22$ for each) were collected to assess FRAP at synapses with high and low levels of tdTom-ELKS1.

Neuron cultures and electrophysiology

Autaptic cultures were prepared as described previously (Jockusch et al., 2007; Burgalossi et al., 2012). bMunc13-2–EGFP variants were expressed using the Semliki Forest virus system. Cells were infected at 10–14 DIV and measured 48 h after infection. Infected cells were identified by their EGFP fluorescence. Sucrose pulse experiments were performed by applying 0.5 M sucrose in standard extracellular solution (Rosenmund and Stevens, 1996). Data are expressed as mean ± SEM. Significance was determined using Student's *t* test.

Subcellular fractionation of mouse cerebral cortex

Cerebral cortices were isolated from mice of the corresponding genotypes, and synaptosome fractions were prepared based on published procedures (Kawabe et al., 2010) with slight modifications. In brief, cortices were homogenized and fractionated by ultracentrifugation using a discontinuous sucrose density gradient. Then, 2.5 mg of purified synaptosomes was incubated in the presence of 1% Triton X-100 at 4°C for 30 min, and the insoluble fraction was sedimented by centrifugation (32,800 *g*, 20 min). The pellet of insoluble material was resuspended in the starting volume of extraction buffer, and identical volumes of soluble and insoluble fractions were separated by SDS-PAGE, transferred to polyvinylidine fluoride or nitrocellulose membranes, and analyzed by Western blotting. Data are expressed as means ± SEM, and significance was determined using Student's *t* test.

Image acquisition, analysis, and statistics

All images for statistical analyses of immunostained brain sections and cultured neurons were acquired with 20×, 40×, or 63× immersion objective lenses using Leica confocal laser scanning microscopes (Leica AOBS SP2 or Leica SP5 equipped with hybrid detectors; Leica Biosystems). Optical sectioning was achieved with a 1 airy unit pinhole setting. The acquisition settings were optimized to avoid underexposure and oversaturation effects and kept equal throughout image acquisition of one set of control vs. mutant samples. Other images were acquired using an Olympus BX61 microscope with 40× or 60× objective lenses. The exposure time was kept identical throughout image acquisition of one set of control versus mutant samples. Signals from cultured neurons for colocalization studies were acquired at Nyquist limit sampling rate and deconvolved by Huygens deconvolution software version 15.1 (Scientific Volume Imaging). All thresholding and analyses were performed with identical settings for a given set of images acquired from control versus mutant samples. Localized Gaussian blur or background subtraction were implemented using IMARIS 8.30 (Bitplane) or Fiji (Schindelin et al., 2012) to reduce noise and/or uneven background signals to ultimately ensure more accurate local maxima detection for spot and mask generation. When centers of two 3D spots were closer than 150 nm in cultured neurons or 200 nm in tissues, they were judged as colocalized spots by IMARIS 8.30 (Bitplane). Alternatively, colocalizing spots were identified with Fiji via pixel-by-pixel multiplication of binarized versions of the two respective stainings. Kaleidagraph (Synergy Software), Instat, or Prism 5 (GraphPad) software was used for statistical analyses. Two independent groups with similar sample numbers were compared with Student's *t* test. More than two groups were compared with one-way analysis of variance test, and Tukey–Kramer multiple comparisons test was applied for comparisons of two groups. Data are expressed as means ± SEM (***, $P < 0.001$; **, $0.001 < P < 0.01$; *, $0.01 < P < 0.05$).

Online supplemental material

Fig. S1 shows data of the FRET analysis of the bMunc13-2–ELKS1 interaction in neurons. Fig. S2 shows the validation of the specificity of antibodies to ELKS1, ELKS2, and bMunc13-2 for immunohistochemical staining. Fig. S3 shows the preferential recruitment of bMunc13-2 to ELKS1 enriched synapses in the hippocampus. Fig. S4 shows data on the degree of colocalization of ELKS1 and Munc13-1 in autaptic hippocampal neurons. Fig. S5 shows data on the expression levels of the bMunc13-2 constructs used for electrophysiological experiments and additional electrophysiological data on the synaptic role of the interaction between bMunc13-2 and ELKS1.

Acknowledgments

We thank B. Hesse-Niessen, K. Hellmann, S. Thiel, I. Thanhäuser, D. Schwerdtfeger, C. Harenberg, M. Schlieper, A. Zeuch, I. Herfort, and H. Deng for excellent technical assistance; the staff of the Max Planck Institute of Experimental Medicine animal facility for maintenance of mouse colonies; A. Schönle for help with his image analysis software, IMSPECTOR; and G. Meyer, F. Benseler, T. Ohtsuka, S. Takamori, A.J. Groffen, D. Trono, L. Naldini, and T. Dresbach for materials, discussions, and advice.

This study was supported by grants from the Deutsche Forschungsgemeinschaft (grant DFG-CNMPB FZT103 to N. Brose, SPP1365/KA3423/1-1 to H. Kawabe and N. Brose, KA3423/3-1 to H. Kawabe, and SFB958/A5 to C. Rosenmund), the European Union (EUROSPIN, SynSys, and European Research Council Advanced Grant SYNPRIME to N. Brose), the National Institutes of Health (grant NS051262 to C. Rosenmund and R01NS083898 to P.S. Kaeser), the Fritz Thyssen Foundation (to H. Kawabe), the Japan Society for the Promotion of Science (to H. Kawabe), and the Mochida Memorial Foundation for Medical and Pharmaceutical Research (to H. Kawabe).

The authors declare no competing financial interests.

Submitted: 6 February 2014
Revised: 18 June 2016
Accepted: 10 January 2017

References

Andrews-Zwilling, Y.S., H. Kawabe, K. Reim, F. Varoqueaux, and N. Brose. 2006. Binding to Rab3A-interacting molecule RIM regulates the presynaptic recruitment of Munc13-1 and ubMunc13-2. *J. Biol. Chem.* 281:19720–19731. http://dx.doi.org/10.1074/jbc.M601421200

Aravamudan, B., and K. Broadie. 2003. Synaptic *Drosophila* UNC-13 is regulated by antagonistic G-protein pathways via a proteasome-dependent degradation mechanism. *J. Neurobiol.* 54:417–438. http://dx.doi.org/10.1002/neu.10142

Augustin, I., A. Betz, C. Herrmann, T. Jo, and N. Brose. 1999a. Differential expression of two novel Munc13 proteins in rat brain. *Biochem. J.* 337:363–371. http://dx.doi.org/10.1042/bj3370363

Augustin, I., C. Rosenmund, T.C. Südhof, and N. Brose. 1999b. Munc13-1 is essential for fusion competence of glutamatergic synaptic vesicles. *Nature.* 400:457–461. http://dx.doi.org/10.1038/22768

Banker, G.A., and W.M. Cowan. 1977. Rat hippocampal neurons in dispersed cell culture. *Brain Res.* 126:397–42. http://dx.doi.org/10.1016/0006-8993(77)90594-7

Bao, J., K. Reim, and T. Sakaba. 2010. Target-dependent feedforward inhibition mediated by short-term synaptic plasticity in the cerebellum. *J. Neurosci.* 30:8171–8179. http://dx.doi.org/10.1523/JNEUROSCI.0276-10.2010

Barde, I., P. Salmon, and D. Trono. 2010. Production and titration of lentiviral vectors. Current Protocols in Neuroscience. Chapter 4:Unit 4.21. https://doi.org/10.1002/0471142301.ns0421s53

Basu, J., N. Shen, I. Dulubova, J. Lu, R. Guan, O. Guryev, N.V. Grishin, C. Rosenmund, and J. Rizo. 2005. A minimal domain responsible for Munc13 activity. *Nat. Struct. Mol. Biol.* 12:1017–1018. http://dx.doi.org/10.1038/nsmb1001

Betz, A., U. Ashery, M. Rickmann, I. Augustin, E. Neher, T.C. Südhof, J. Rettig, and N. Brose. 1998. Munc13-1 is a presynaptic phorbol ester receptor that enhances neurotransmitter release. *Neuron.* 21:123–136. http://dx.doi.org/10.1016/S0896-6273(00)80520-6

Betz, A., P. Thakur, H.J. Junge, U. Ashery, J.S. Rhee, V. Scheuss, C. Rosenmund, J. Rettig, and N. Brose. 2001. Functional interaction of the active zone proteins Munc13-1 and RIM1 in synaptic vesicle priming. *Neuron.* 30:183–196. http://dx.doi.org/10.1016/S0896-6273(01)00272-0

Böhme, M.A., C. Beis, S. Reddy-Alla, E. Reynolds, M.M. Mampell, A.T. Grasskamp, J. Lützkendorf, D.D. Bergeron, J.H. Driller, H. Babikir, et al. 2016. Active zone scaffolds differentially accumulate Unc13 isoforms to tune Ca(2+) channel-vesicle coupling. *Nat. Neurosci.* 19:1311–1320. http://dx.doi.org/10.1038/nn.4364

Breustedt, J., A. Gundlfinger, F. Varoqueaux, K. Reim, N. Brose, and D. Schmitz. 2010. Munc13-2 differentially affects hippocampal synaptic transmission and plasticity. *Cereb. Cortex.* 20:1109–1120. http://dx.doi.org/10.1093/cercor/bhp170

Brose, N., K. Hofmann, Y. Hata, and T.C. Südhof. 1995. Mammalian homologues of *Caenorhabditis elegans* unc-13 gene define novel family of C2-domain proteins. *J. Biol. Chem.* 270:25273–25280. http://dx.doi.org/10.1074/jbc.270.42.25273

Burgalossi, A., S. Jung, K.N. Man, R. Nair, W.J. Jockusch, S.M. Wojcik, N. Brose, and J.S. Rhee. 2012. Analysis of neurotransmitter release mechanisms by photolysis of caged Ca^{2+} in an autaptic neuron culture system. *Nat. Protoc.* 7:1351–1365. http://dx.doi.org/10.1038/nprot.2012.074

Calakos, N., S. Schoch, T.C. Südhof, and R.C. Malenka. 2004. Multiple roles for the active zone protein RIM1alpha in late stages of neurotransmitter release. *Neuron.* 42:889–896. http://dx.doi.org/10.1016/j.neuron.2004.05.014

Castillo, P.E., S. Schoch, F. Schmitz, T.C. Südhof, and R.C. Malenka. 2002. RIM1alpha is required for presynaptic long-term potentiation. *Nature.* 415:327–330. http://dx.doi.org/10.1038/415327a

Cooper, B., M. Hemmerlein, J. Ammermüller, C. Imig, K. Reim, N. Lipstein, S. Kalla, H. Kawabe, N. Brose, J.H. Brandstätter, and F. Varoqueaux. 2012. Munc13-independent vesicle priming at mouse photoreceptor ribbon synapses. *J. Neurosci.* 32:8040–8052. http://dx.doi.org/10.1523/JNEUROSCI.4240-11.2012

Dai, Y., H. Taru, S.L. Deken, B. Grill, B. Ackley, M.L. Nonet, and Y. Jin. 2006. SYD-2 Liprin-alpha organizes presynaptic active zone formation through ELKS. *Nat. Neurosci.* 9:1479–1487. http://dx.doi.org/10.1038/nn1808

Deguchi-Tawarada, M., E. Inoue, E. Takao-Rikitsu, M. Inoue, T. Ohtsuka, and Y. Takai. 2004. CAST2: Identification and characterization of a protein structurally related to the presynaptic cytomatrix protein CAST. *Genes Cells.* 9:15–23. http://dx.doi.org/10.1111/j.1356-9597.2004.00697.x

Deken, S.L., R. Vincent, G. Hadwiger, Q. Liu, Z.W. Wang, and M.L. Nonet. 2005. Redundant localization mechanisms of RIM and ELKS in Caenorhabditis elegans. *J. Neurosci.* 25:5975–5983. http://dx.doi.org/10.1523/JNEUROSCI.0804-05.2005

Deng, L., P.S. Kaeser, W. Xu, and T.C. Südhof. 2011. RIM proteins activate vesicle priming by reversing autoinhibitory homodimerization of Munc13. *Neuron.* 69:317–331. http://dx.doi.org/10.1016/j.neuron.2011.01.005

DiCiommo, D.P., and R. Bremner. 1998. Rapid, high level protein production using DNA-based Semliki Forest virus vectors. *J. Biol. Chem.* 273:18060–18066. http://dx.doi.org/10.1074/jbc.273.29.18060

Dresbach, T., A. Hempelmann, C. Spilker, S. tom Dieck, W.D. Altrock, W. Zuschratter, C.C. Garner, and E.D. Gundelfinger. 2003. Functional regions of the presynaptic cytomatrix protein bassoon: Significance for synaptic targeting and cytomatrix anchoring. *Mol. Cell. Neurosci.* 23:279–291. http://dx.doi.org/10.1016/S1044-7431(03)00015-0

Dulubova, I., X. Lou, J. Lu, I. Huryeva, A. Alam, R. Schneggenburger, T.C. Südhof, and J. Rizo. 2005. A Munc13/RIM/Rab3 tripartite complex: from priming to plasticity? *EMBO J.* 24:2839–2850. http://dx.doi.org/10.1038/sj.emboj.7600753

Fenster, S.D., W.J. Chung, R. Zhai, C. Cases-Langhoff, B. Voss, A.M. Garner, U. Kaempf, S. Kindler, E.D. Gundelfinger, and C.C. Garner. 2000. Piccolo, a presynaptic zinc finger protein structurally related to bassoon. *Neuron.* 25:203–214. http://dx.doi.org/10.1016/S0896-6273(00)80883-1

Fernández-Busnadiego, R., S. Asano, A.M. Oprisoreanu, E. Sakata, M. Doengi, Z. Kochovski, M. Zürner, V. Stein, S. Schoch, W. Baumeister, and V. Lučić. 2013. Cryo-electron tomography reveals a critical role of RIM1α in synaptic vesicle tethering. *J. Cell Biol.* 201:725–740. http://dx.doi.org/10.1083/jcb.201206063

Follenzi, A., and L. Naldini. 2002. HIV-based vectors. Preparation and use. *Methods Mol. Med.* 69:259–274.

Gorski, J.A., T. Talley, M. Qiu, L. Puelles, J.L. Rubenstein, and K.R. Jones. 2002. Cortical excitatory neurons and glia, but not GABAergic neurons, are produced in the Emx1-expressing lineage. *J. Neurosci.* 22:6309–6314.

Hagiwara, A., Y. Fukazawa, M. Deguchi-Tawarada, T. Ohtsuka, and R. Shigemoto. 2005. Differential distribution of release-related proteins in the hippocampal CA3 area as revealed by freeze-fracture replica labeling. *J. Comp. Neurol.* 489:195–216. http://dx.doi.org/10.1002/cne.20633

Han, Y., P.S. Kaeser, T.C. Südhof, and R. Schneggenburger. 2011. RIM determines Ca^{2}+ channel density and vesicle docking at the presynaptic active zone. *Neuron.* 69:304–316. http://dx.doi.org/10.1016/j.neuron.2010.12.014

Held, R.G., C. Liu, and P.S. Kaeser. 2016. ELKS controls the pool of readily releasable vesicles at excitatory synapses through its N-terminal coiled-coil domains. *eLife.* 5:e114862. http://dx.doi.org/10.7554/eLife.14862

Hsia, H.E., R. Kumar, R. Luca, M. Takeda, J. Courchet, J. Nakashima, S. Wu, S. Goebbels, W. An, B.J. Eickholt, et al. 2014. Ubiquitin E3 ligase Nedd4-1 acts as a downstream target of PI3K/PTEN-mTORC1 signaling to promote neurite growth. *Proc. Natl. Acad. Sci. USA*. 111:13205–13210. http://dx.doi.org/10.1073/pnas.1400737111

Hu, Z., X.J. Tong, and J.M. Kaplan. 2013. UNC-13L, UNC-13S, and Tomosyn form a protein code for fast and slow neurotransmitter release in *Caenorhabditis elegans*. *eLife.* 2:e00967. http://dx.doi.org/10.7554/eLife.00967

James, P., J. Halladay, and E.A. Craig. 1996. Genomic libraries and a host strain designed for highly efficient two-hybrid selection in yeast. *Genetics.* 144:1425–1436.

Jockusch, W.J., D. Speidel, A. Sigler, J.B. Sørensen, F. Varoqueaux, J.S. Rhee, and N. Brose. 2007. CAPS-1 and CAPS-2 are essential synaptic vesicle priming proteins. *Cell.* 131:796–808. http://dx.doi.org/10.1016/j.cell.2007.11.002

Junge, H.J., J.S. Rhee, O. Jahn, F. Varoqueaux, J. Spiess, M.N. Waxham, C. Rosenmund, and N. Brose. 2004. Calmodulin and Munc13 form a Ca2+ sensor/effector complex that controls short-term synaptic plasticity. *Cell.* 118:389–401. http://dx.doi.org/10.1016/j.cell.2004.06.029

Kaeser, P.S., H.B. Kwon, C.Q. Chiu, L. Deng, P.E. Castillo, and T.C. Südhof. 2008. RIM1alpha and RIM1beta are synthesized from distinct promoters of the RIM1 gene to mediate differential but overlapping synaptic functions. *J. Neurosci.* 28:13435–13447. http://dx.doi.org/10.1523/JNEUROSCI.3235-08.2008

Kaeser, P.S., L. Deng, A.E. Chávez, X. Liu, P.E. Castillo, and T.C. Südhof. 2009. ELKS2alpha/CAST deletion selectively increases neurotransmitter release at inhibitory synapses. *Neuron.* 64:227–239. http://dx.doi.org/10.1016/j.neuron.2009.09.019

Kaeser, P.S., L. Deng, Y. Wang, I. Dulubova, X. Liu, J. Rizo, and T.C. Südhof. 2011. RIM proteins tether Ca2+ channels to presynaptic active zones via a direct PDZ-domain interaction. *Cell.* 144:282–295. http://dx.doi.org/10.1016/j.cell.2010.12.029

Kalla, S., M. Stern, J. Basu, F. Varoqueaux, K. Reim, C. Rosenmund, N.E. Ziv, and N. Brose. 2006. Molecular dynamics of a presynaptic active zone protein studied in Munc13-1-enhanced yellow fluorescent protein knock-in mutant mice. *J. Neurosci.* 26:13054–13066. http://dx.doi.org/10.1523/JNEUROSCI.4330-06.2006

Kawabe, H., A. Neeb, K. Dimova, S.M. Young Jr., M. Takeda, S. Katsurabayashi, M. Mitkovski, O.A. Malakhova, D.E. Zhang, M. Umikawa, et al. 2010. Regulation of Rap2A by the ubiquitin ligase Nedd4-1 controls neurite development. *Neuron.* 65:358–372. http://dx.doi.org/10.1016/j.neuron.2010.01.007

Kittel, R.J., C. Wichmann, T.M. Rasse, W. Fouquet, M. Schmidt, A. Schmid, D.A. Wagh, C. Pawlu, R.R. Kellner, K.I. Willig, et al. 2006. Bruchpilot promotes active zone assembly, Ca2+ channel clustering, and vesicle release. *Science.* 312:1051–1054. http://dx.doi.org/10.1126/science.1126308

Kiyonaka, S., M. Wakamori, T. Miki, Y. Uriu, M. Nonaka, H. Bito, A.M. Beedle, E. Mori, Y. Hara, M. De Waard, et al. 2007. RIM1 confers sustained activity and neurotransmitter vesicle anchoring to presynaptic Ca2+ channels. *Nat. Neurosci.* 10:691–701. http://dx.doi.org/10.1038/nn1904

Ko, J., M. Na, S. Kim, J.R. Lee, and E. Kim. 2003. Interaction of the ERC family of RIM-binding proteins with the liprin-alpha family of multidomain proteins. *J. Biol. Chem.* 278:42377–42385. http://dx.doi.org/10.1074/jbc.M307561200

Koch, H., K. Hofmann, and N. Brose. 2000. Definition of Munc13-homology-domains and characterization of a novel ubiquitously expressed Munc13 isoform. *Biochem. J.* 349:247–253. http://dx.doi.org/10.1042/bj3490247

Kohn, R.E., J.S. Duerr, J.R. McManus, A. Duke, T.L. Rakow, H. Maruyama, G. Moulder, I.N. Maruyama, R.J. Barstead, and J.B. Rand. 2000. Expression of multiple UNC-13 proteins in the *Caenorhabditis elegans* nervous system. *Mol. Biol. Cell.* 11:3441–3452. http://dx.doi.org/10.1091/mbc.11.10.3441

Koushika, S.P., J.E. Richmond, G. Hadwiger, R.M. Weimer, E.M. Jorgensen, and M.L. Nonet. 2001. A post-docking role for active zone protein Rim. *Nat. Neurosci.* 4:997–1005. http://dx.doi.org/10.1038/nn732

Liu, C., L.S. Bickford, R.G. Held, H. Nyitrai, T.C. Südhof, and P.S. Kaeser. 2014. The active zone protein family ELKS supports Ca2+ influx at nerve terminals of inhibitory hippocampal neurons. *J. Neurosci.* 34:12289–12303. http://dx.doi.org/10.1523/JNEUROSCI.0999-14.2014

Lois, C., E.J. Hong, S. Pease, E.J. Brown, and D. Baltimore. 2002. Germline transmission and tissue-specific expression of transgenes delivered by lentiviral vectors. *Science.* 295:868–872. http://dx.doi.org/10.1126/science.1067081

Ma, C., L. Su, A.B. Seven, Y. Xu, and J. Rizo. 2013. Reconstitution of the vital functions of Munc18 and Munc13 in neurotransmitter release. *Science.* 339:421–425. http://dx.doi.org/10.1126/science.1230473

Mochida, S., Y. Hida, S. Tanifuji, A. Hagiwara, S. Hamada, M. Abe, H. Ma, M. Yasumura, I. Kitajima, K. Sakimura, and T. Ohtsuka. 2016. SAD-B phosphorylation of CAST controls active zone vesicle recycling for synaptic depression. *Cell Reports.* 16:2901–2913. http://dx.doi.org/10.1016/j.celrep.2016.08.020

Monier, S., F. Jollivet, I. Janoueix-Lerosey, L. Johannes, and B. Goud. 2002. Characterization of novel Rab6-interacting proteins involved in endosome-to-TGN transport. *Traffic.* 3:289–297. http://dx.doi.org/10.1034/j.1600-0854.2002.030406.x

Nakata, T., Y. Kitamura, K. Shimizu, S. Tanaka, M. Fujimori, S. Yokoyama, K. Ito, and M. Emi. 1999. Fusion of a novel gene, ELKS, to RET due to translocation t(10;12)(q11;p13) in a papillary thyroid carcinoma. *Genes Chromosomes Cancer.* 25:97–103. http://dx.doi.org/10.1002/(SICI)1098-2264(199906)25:2<97::AID-GCC4>3.0.CO;2-L

Neculai, D., A.M. Neculai, S. Verrier, K. Straub, K. Klumpp, E. Pfitzner, and S. Becker. 2005. Structure of the unphosphorylated STAT5a dimer. *J. Biol. Chem.* 280:40782–40787. http://dx.doi.org/10.1074/jbc.M507682200

Nurrish, S., L. Ségalat, and J.M. Kaplan. 1999. Serotonin inhibition of synaptic transmission: Galpha(0) decreases the abundance of UNC-13 at release sites. *Neuron.* 24:231–242. http://dx.doi.org/10.1016/S0896-6273(00)80835-1

Ohtsuka, T., E. Takao-Rikitsu, E. Inoue, M. Inoue, M. Takeuchi, K. Matsubara, M. Deguchi-Tawarada, K. Satoh, K. Morimoto, H. Nakanishi, and Y. Takai. 2002. Cast: A novel protein of the cytomatrix at the active zone of synapses that forms a ternary complex with RIM1 and munc13-1. *J. Cell Biol.* 158:577–590. http://dx.doi.org/10.1083/jcb.200202083

Reyes, A., R. Lujan, A. Rozov, N. Burnashev, P. Somogyi, and B. Sakmann. 1998. Target-cell-specific facilitation and depression in neocortical circuits. *Nat. Neurosci.* 1:279–285. http://dx.doi.org/10.1038/1092

Rhee, J.S., A. Betz, S. Pyott, K. Reim, F. Varoqueaux, I. Augustin, D. Hesse, T.C. Südhof, M. Takahashi, C. Rosenmund, and N. Brose. 2002. Beta phorbol ester- and diacylglycerol-induced augmentation of transmitter release is mediated by Munc13s and not by PKCs. *Cell.* 108:121–133. http://dx.doi.org/10.1016/S0092-8674(01)00635-3

Richmond, J.E., R.M. Weimer, and E.M. Jorgensen. 2001. An open form of syntaxin bypasses the requirement for UNC-13 in vesicle priming. *Nature.* 412:338–341. http://dx.doi.org/10.1038/35085583

Rosenmund, C., and C.F. Stevens. 1996. Definition of the readily releasable pool of vesicles at hippocampal synapses. *Neuron.* 16:1197–1207. http://dx.doi.org/10.1016/S0896-6273(00)80146-4

Rosenmund, C., A. Sigler, I. Augustin, K. Reim, N. Brose, and J.S. Rhee. 2002. Differential control of vesicle priming and short-term plasticity by Munc13 isoforms. *Neuron.* 33:411–424. http://dx.doi.org/10.1016/S0896-6273(02)00568-8

Rosenmund, C., J. Rettig, and N. Brose. 2003. Molecular mechanisms of active zone function. *Curr. Opin. Neurobiol.* 13:509–519. http://dx.doi.org/10.1016/j.conb.2003.09.011

Schindelin, J., I. Arganda-Carreras, E. Frise, V. Kaynig, M. Longair, T. Pietzsch, S. Preibisch, C. Rueden, S. Saalfeld, B. Schmid, et al. 2012. Fiji: An open-source platform for biological-image analysis. *Nat. Methods.* 9:676–682. http://dx.doi.org/10.1038/nmeth.2019

Schoch, S., P.E. Castillo, T. Jo, K. Mukherjee, M. Geppert, Y. Wang, F. Schmitz, R.C. Malenka, and T.C. Südhof. 2002. RIM1alpha forms a protein scaffold for regulating neurotransmitter release at the active zone. *Nature.* 415:321–326. http://dx.doi.org/10.1038/415321a

Schoch, S., T. Mittelstaedt, P.S. Kaeser, D. Padgett, N. Feldmann, V. Chevaleyre, P.E. Castillo, R.E. Hammer, W. Han, F. Schmitz, et al. 2006. Redundant functions of RIM1alpha and RIM2alpha in Ca(2+)-triggered neurotransmitter release. *EMBO J.* 25:5852–5863. http://dx.doi.org/10.1038/sj.emboj.7601425

Serra-Pagès, C., Q.G. Medley, M. Tang, A. Hart, and M. Streuli. 1998. Liprins, a family of LAR transmembrane protein-tyrosine phosphatase-interacting proteins. *J. Biol. Chem.* 273:15611–15620. http://dx.doi.org/10.1074/jbc.273.25.15611

Shapira, M., R.G. Zhai, T. Dresbach, T. Bresler, V.I. Torres, E.D. Gundelfinger, N.E. Ziv, and C.C. Garner. 2003. Unitary assembly of presynaptic active zones from Piccolo-Bassoon transport vesicles. *Neuron.* 38:237–252. http://dx.doi.org/10.1016/S0896-6273(03)00207-1

Shin, O.H., J. Lu, J.S. Rhee, D.R. Tomchick, Z.P. Pang, S.M. Wojcik, M. Camacho-Perez, N. Brose, M. Machius, J. Rizo, et al. 2010. Munc13 C2B domain is an activity-dependent Ca2+ regulator of synaptic exocytosis. *Nat. Struct. Mol. Biol.* 17:280–288. http://dx.doi.org/10.1038/nsmb.1758

Siksou, L., P. Rostaing, J.P. Lechaire, T. Boudier, T. Ohtsuka, A. Fejtová, H.T. Kao, P. Greengard, E.D. Gundelfinger, A. Triller, and S. Marty. 2007. Three-dimensional architecture of presynaptic terminal cytomatrix. *J. Neurosci.* 27:6868–6877. http://dx.doi.org/10.1523/JNEUROSCI.1773-07.2007

Spangler, S.A., S.K. Schmitz, J.T. Kevenaar, E. de Graaff, H. de Wit, J. Demmers, R.F. Toonen, and C.C. Hoogenraad. 2013. Liprin-α2 promotes the presynaptic recruitment and turnover of RIM1/CASK to facilitate synaptic transmission. *J. Cell Biol.* 201:915–928. http://dx.doi.org/10.1083/jcb.201301011

Speese, S.D., N. Trotta, C.K. Rodesch, B. Aravamudan, and K. Broadie. 2003. The ubiquitin proteasome system acutely regulates presynaptic protein turnover and synaptic efficacy. *Curr. Biol.* 13:899–910. http://dx.doi.org/10.1016/S0960-9822(03)00338-5

Stevens, D.R., Z.X. Wu, U. Matti, H.J. Junge, C. Schirra, U. Becherer, S.M. Wojcik, N. Brose, and J. Rettig. 2005. Identification of the minimal protein domain required for priming activity of Munc13-1. *Curr. Biol.* 15:2243–2248. http://dx.doi.org/10.1016/j.cub.2005.10.055

Südhof, T.C. 2012. The presynaptic active zone. *Neuron.* 75:11–25. http://dx.doi.org/10.1016/j.neuron.2012.06.012

Takahashi, H., P. Arstikaitis, T. Prasad, T.E. Bartlett, Y.T. Wang, T.H. Murphy, and A.M. Craig. 2011. Postsynaptic TrkC and presynaptic PTPσ function as a bidirectional excitatory synaptic organizing complex. *Neuron.* 69:287–303. http://dx.doi.org/10.1016/j.neuron.2010.12.024

Takao-Rikitsu, E., S. Mochida, E. Inoue, M. Deguchi-Tawarada, M. Inoue, T. Ohtsuka, and Y. Takai. 2004. Physical and functional interaction of the active zone proteins, CAST, RIM1, and Bassoon, in neurotransmitter release. *J. Cell Biol.* 164:301–311. http://dx.doi.org/10.1083/jcb.200307101

tom Dieck, S., L. Sanmartí-Vila, K. Langnaese, K. Richter, S. Kindler, A. Soyke, H. Wex, K.H. Smalla, U. Kämpf, J.T. Fränzer, et al. 1998. Bassoon, a novel zinc-finger CAG/glutamine-repeat protein selectively localized at the active zone of presynaptic nerve terminals. *J. Cell Biol.* 142:499–509. http://dx.doi.org/10.1083/jcb.142.2.499

tom Dieck, S., D. Specht, N. Strenzke, Y. Hida, V. Krishnamoorthy, K.F. Schmidt, E. Inoue, H. Ishizaki, M. Tanaka-Okamoto, J. Miyoshi, et al. 2012. Deletion of the presynaptic scaffold CAST reduces active zone size in rod photoreceptors and impairs visual processing. *J. Neurosci.* 32:12192–12203. http://dx.doi.org/10.1523/JNEUROSCI.0752-12.2012

Varoqueaux, F., A. Sigler, J.S. Rhee, N. Brose, C. Enk, K. Reim, and C. Rosenmund. 2002. Total arrest of spontaneous and evoked synaptic transmission but normal synaptogenesis in the absence of Munc13-mediated vesicle priming. *Proc. Natl. Acad. Sci. USA.* 99:9037–9042. http://dx.doi.org/10.1073/pnas.122623799

Verrier, S.E., M. Willmann, D. Wenzel, U. Winter, G.F. von Mollard, and H.D. Söling. 2008. Members of a mammalian SNARE complex interact in the endoplasmic reticulum in vivo and are found in COPI vesicles. *Eur. J. Cell Biol.* 87:863–878. http://dx.doi.org/10.1016/j.ejcb.2008.07.003

Wagh, D.A., T.M. Rasse, E. Asan, A. Hofbauer, I. Schwenkert, H. Dürrbeck, S. Buchner, M.C. Dabauvalle, M. Schmidt, G. Qin, et al. 2006. Bruchpilot, a protein with homology to ELKS/CAST, is required for structural integrity and function of synaptic active zones in Drosophila. *Neuron.* 49:833–844. http://dx.doi.org/10.1016/j.neuron.2006.02.008

Wang, X., M. Kibschull, M.M. Laue, B. Lichte, E. Petrasch-Parwez, and M.W. Kilimann. 1999. Aczonin, a 550-kD putative scaffolding protein of presynaptic active zones, shares homology regions with Rim and Bassoon and binds profilin. *J. Cell Biol.* 147:151–162. http://dx.doi.org/10.1083/jcb.147.1.151

Wang, Y., M. Okamoto, F. Schmitz, K. Hofmann, and T.C. Südhof. 1997. Rim is a putative Rab3 effector in regulating synaptic-vesicle fusion. *Nature.* 388:593–598. http://dx.doi.org/10.1038/41580

Wang, Y., X. Liu, T. Biederer, and T.C. Südhof. 2002. A family of RIM-binding proteins regulated by alternative splicing: Implications for the genesis of synaptic active zones. *Proc. Natl. Acad. Sci. USA.* 99:14464–14469. http://dx.doi.org/10.1073/pnas.182532999

Wojcik, S.M., and N. Brose. 2007. Regulation of membrane fusion in synaptic excitation-secretion coupling: Speed and accuracy matter. *Neuron.* 55:11–24. http://dx.doi.org/10.1016/j.neuron.2007.06.013

Yang, X., S. Wang, Y. Sheng, M. Zhang, W. Zou, L. Wu, L. Kang, J. Rizo, R. Zhang, T. Xu, and C. Ma. 2015. Syntaxin opening by the MUN domain underlies the function of Munc13 in synaptic-vesicle priming. *Nat. Struct. Mol. Biol.* 22:547–554. http://dx.doi.org/10.1038/nsmb.3038

Zikich, D., A. Mezer, F. Varoqueaux, A. Sheinin, H.J. Junge, E. Nachliel, R. Melamed, N. Brose, M. Gutman, and U. Ashery. 2008. Vesicle priming and recruitment by ubMunc13-2 are differentially regulated by calcium and calmodulin. *J. Neurosci.* 28:1949–1960. http://dx.doi.org/10.1523/JNEUROSCI.5096-07.2008

Zürner, M., and S. Schoch. 2009. The mouse and human Liprin-alpha family of scaffolding proteins: Genomic organization, expression profiling and regulation by alternative splicing. *Genomics.* 93:243–253. http://dx.doi.org/10.1016/j.ygeno.2008.10.007